University of Crete
Department of Physics

CERN
BE-ABP-HSI

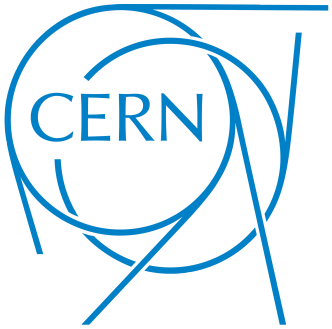

Master's Thesis in Advanced Physics

Chaos Map Analysis of Particle Stability in Accelerators

Author: Michail Zampetakis
E-mail: mzampetakis@physics.uoc.gr

Supervisor: Dr. Frank Schmidt
E-mail: frank.schmidt@cern.ch

Academic Supervisor: Prof. Theodore Tomaras
E-mail: tomaras@physics.uoc.gr

Heraklion, October 1, 2018

Abstract

It is well known that the combination of Space charge and lattice imperfections can put the beam stability at stake when it has to survive for a large number of turns. In such cases, particles may exhibit chaotic motion leading to particle losses and beam blow-up. Therefore, tools that predict at which amplitudes the particle motion becomes chaotic are always useful. There are already tools of such use, like Frequency Map Analysis. In this study, the newly developed tool, Chaos Map Analysis, will be reviewed and compared with the former. Instead of determining the chaotic behaviour of particles with tune diffusion, the Chaos Map Analysis method takes advantage of the phase-space-difference evolution between two particles presenting visual results onto a 6D amplitude grid. The results of this study show that the Chaos Map Analysis method is in great agreement with the Frequency Map Analysis.

Nomenclature

Acronyms

CERN	-European Organization for Nuclear Research
PS	-CERN Proton Synchrotron
LHC	-CERN Large Hadron Collider
FMA	-Frequency Map Analysis
CMA	-Chaos Map Analysis
SC	-Space Charge
WP	-Working Point
DOF	-Degree of Freedom
FFT	-Fast Fourier Transform
MAD	-Methodical Accelerator Design

Constants

c	-Speed of light, $[3 \times 10^8 m/s]$
m_0	-Proton mass, $[1.673 \times 10^{-27}\text{kg}]$
e	-Elementary charge, $[1.602 \times 10^{-19}\text{C}]$
r_0	-Classical radius, $[1.54 \times 10^{-18}\text{m}$ (protons)$]$
ε_0	-Vacuum permittivity, $[8.854 \times 10^{-12}$ F/m$]$

Acknowledgments

I would like to express my gratitude to my supervisor Dr. Frank Schmidt from CERN, for his useful comments, patience, motivation, and immense knowledge. His willingness to give his time so generously trying to explain all these complex concepts to me has been very much appreciated and without his precious support it would not be possible to conduct this research.

I wish to acknowledge my academic supervisor Prof. Theodore Tomaras from the University of Crete, who encouraged me to apply to do my master thesis at CERN and made all the procedures of the university easy for me.

I am particularly grateful for the assistance given by Dr. Yannis Papaphilippou from CERN, on improving the FMA method for this particular study. In addition, I would like to thank all my colleagues Foteini, Natalia, Vasilis, Sofia, Daniel, Stefania, Kyriacos, Loizos and Despoina for all the assistance they have provided me with and all the fun we had.

Finally, I would like to express my profound gratitude to my family and my friends from Crete for providing me with unfailing support throughout this year of researching and writing this thesis.

Author

Michail Zampetakis

Contents

1 Introduction **1**

2 Theory and Background **2**
2.1 Betatron Tunes . . . 2
2.1.1 Periodic Solutions . . . 3
2.2 Resonances . . . 5
2.2.1 Conditions of Coupling Resonances . . . 5
2.3 Space Charge . . . 7
2.3.1 Direct Space Charge . . . 7
2.3.2 Direct *SC*: Incoherent Tune Shift . . . 8
2.3.3 A visual example . . . 9
2.4 Chaos . . . 10
2.4.1 Deterministic Chaos . . . 10
2.4.2 The Lyapunov Exponent . . . 11
2.5 Frequency Map Analysis . . . 11
2.5.1 Frequency analysis . . . 11
2.5.2 Maps creation and Diffusion estimation . . . 12

3 CMA Tool - Description **14**
3.1 Tools . . . 15
3.2 CMA Parameters . . . 15
3.3 CMA Technique . . . 17
3.3.1 Simulation Set-up . . . 17
3.3.2 Data Analysis . . . 18
3.3.3 Angular Distance in Phase Space . . . 18
3.3.4 Chaos Characterization . . . 21

4 CMA - Benchmarking **24**

5 Toy Model **26**
5.1 Resonance Tune . . . 27

6 PS **29**
6.1 Safe Tune . . . 30
6.2 Resonance Tune . . . 32
6.2.1 Frozen Mode . . . 34
6.3 Integer Tune . . . 37

7 Conclusions **39**

A : Benchmarking Plots **40**

1 Introduction

In this Thesis, the subject is to investigate particle stability in storage rings. To this end, the CERN Proton Synchrotron (PS) is taken as an example where particles have to survive for long times, ie. for many number of passes through the machine, called number of turns.

Single particle stability is limited by non-linear elements that may be required for either machine control, e.g. chromaticity correction, or through unwanted magnet imperfections. There are also various collective effects that may lead to instabilities of particle bunches. In this study only *Direct Space Charge* (SC) will be considered.

If the non-linearities are significantly strong, they will lead to chaotic motion within the physical aperture of the beam. It is well-known[1] that particles that exhibit chaotic behaviour are found at large transverse oscillation amplitudes and are eventually lost as off a certain amplitude in phase space. In particular for small storage rings like the PS ($628m$) and at injection energy, the SC effect of large intensity beams cannot be ignored. SC in conjunction with the non-linearities may lead to beam blow-up and losses as well. Even without non-linearities, though, SC can create resonances on its own.

The goal of this study is to review present tools (*Frequency Map Analysis*, or FMA in short) and a newly developed tool (*Chaos Map Analysis*, or CMA in short) to predict at which amplitudes particle motion becomes chaotic leading to beam blow-up or particle losses. For several tune working points (WPs) for the PS, the particle stability is presented onto a 6D amplitude grid such that the amplitude at which motion becomes chaotic can be visually identified.

The difficulty of the grid implementation is that we are dealing with a phase space in 6D. The most relevant information is to find the strength of resonances in the transverse planes. Therefore, amplitudes in the transverse planes are sampled in 0.5 sigma steps and 5 ratios of the horizontal and vertical emittances are used. In the longitudinal phase space 3 P_t values are chosen for $0.02\sigma_l$, $1\sigma_l$ and $2\sigma_l$. For the smallest P_t value, the motion is mainly transverse, while for $P_t = 1\sigma_l$ is at the limit of the beam center. Last, at $2\sigma_l$ one samples the edge of the longitudinal distribution.

It is well know that the strength of the resonances depend on the tunes rather than phase advances which may vary strongly. In 6D typically the longitudinal tune Q_s is very small, meaning that the synchrotron period is very large. On the other hand, the transverse tunes depend longitudinally, linearly and even non-linearly on P_t. Therefore, it is required to determine the 6D tunes over a full number of synchrotron periods for a reliable evaluation of the effect resonances have on the beam. It is interesting to note that a similar argument holds also for power supply ripple. Again, one needs to determine the tunes over full ripple periods.

The CMA technique required a reliable measure of when the particle motion is regular or chaotic. Strong chaotic behaviour can easily be identified by strongly chaotic motion in the phase space. The problem is to distinguish truly regular from only weakly chaotic motion. This will be discussed in the thesis and benchmarked with the number of synchrotron periods required to minimize the error in determining the onset of chaotic motion.

2 Theory and Background

To this end, some theory needs to be briefly discussed in order to build a basic background and better understand some concepts that are related to this project. These concepts are the *Betatron Tunes* which are frequencies that particles oscillate transversely. The *Resonances* which are a major issue that leads to particle losses and sometimes to chaotic behavior. *Space Charge* which is a collective effect that causes the tunes to spread and in that way the particles to cross resonances. Also, *Chaos* will be briefly mentioned to have an idea about what we study and last, the *FMA* method, which is the method that will be reviewed and compared with the newly developed CMA method.

2.1 Betatron Tunes

The basis of the calculations in linear beam optics[2] are formed by the following two equations

$$x''(s) + \left(\frac{1}{R^2(s)} - k(s)\right) x(s) = \frac{1}{R(s)} \frac{\Delta p}{p} \tag{1}$$

$$y''(s) + k(s) y(s) = 0 \tag{2}$$

with $R(s)$ being the bending radius and $k(s)$ the quadrupole strength. These two equations are the equations of motion for a particle traveling through the magnetic structure of an accelerator. These two coordinates represent the transverse plane of the beam. The extra terms in the horizontal plane comes from the bending magnets that do not take place in the vertical plane.

If one desires to describe the behavior of the entire composite beam, it has to be assumed that the bending radius is very large so as $1/R^2(s) = 0$ and the particles are "*on-momentum*", so as $\Delta p/p = 0$. By doing that, the horizontal plane's equation takes the form of the Hill's differential equation of motion

$$x''(s) - k(s) x(s) = 0 \tag{3}$$

The trajectory function $x(s)$ describes a transverse oscillation about the orbit, know as a **betatron oscillation**, whose amplitude and phase depend on the position s along the orbit. Therefore, one can solve the equation (3) by using the trial solution

$$x(s) = A\, u(s)\, \cos[\Psi(s) + \phi] \tag{4}$$

with the constant amplitude factor A and the phase ϕ being constants of integration which are fixed by the initial conditions. Inserting (4) and its second derivative into (3) and simplifying $u(s)$ to u and $\Psi(s)$ to Ψ, one can get

$$A\big[u'' - u\Psi'^2 - k(s)u\big] \cos(\Psi + \phi) - A\big[2u'\Psi' + u\Psi''\big] \sin(\Psi + \phi) = 0 \tag{5}$$

Though, A is always non-zero and $\Psi(s)$ takes different values around the orbit, so the only way to satisfy equation (5) is when

$$u'' - u\Psi'^2 - k(s)u = 0 \tag{6}$$

$$2u'\Psi' + u\Psi'' = 0 \tag{7}$$

From equation (7) follows that

$$2\frac{u'}{u} + \frac{\Psi''}{\Psi'} = 0 \tag{8}$$

which can be integrated directly, giving

$$\Psi(s) = \int_0^s \frac{ds}{u^2(s)}. \tag{9}$$

By inserting this result into (6), follows

$$u'' - \frac{1}{u^3} - k(s)u = 0 \tag{10}$$

which is a non-linear differential equation with no general analytic solution. It may be evaluated only by numerical methods which is hardly practical when we have complicated magnet structures with many individual elements. In order to make things clearer and with some meaning, we introduce the **beta function** $\beta(s)$, also known as **amplitude function**. Is is defined as

$$\beta(s) \equiv u^2(s). \tag{11}$$

Furthermore, the amplitude factor A is replaced by $\sqrt{\varepsilon}$. The constant ϵ is termed the **emittance** of the beam. Finally, we can write the solution of the trajectory equation (3) in the following form

$$x(s) = \sqrt{\varepsilon}\sqrt{\beta(s)}\,\cos[\Psi(s) + \phi] \tag{12}$$

with

$$\Psi(s) = \int_0^s \frac{ds}{\beta(s)}. \tag{13}$$

Withing the focusing effect of the magnet structure, the particles perform betatron oscillations with an amplitude that depends on their position. This amplitude is given by

$$E(s) = \sqrt{\varepsilon\beta(s)} \tag{14}$$

and forms the envelope of the beam as can be seen in the Figure (2.1).

2.1.1 Periodic Solutions

In circular accelerators such as synchrotrons or storage rings, the beam repeatedly experiences the same magnet structure on every turn. Namely, the forces that the beam encounters are periodic.

Again the Hill's differential equation for "*on-momentum*" particles is

$$x''(s) + K(s)x(s) = 0. \tag{15}$$

As was previously shown, the focusing function is $K(s) = 1/R(s) - k(s)$ and in a circular machine case, it is periodic with the circumference of the ring L:

$$K(s + L) = K(s) \tag{16}$$

Using Floquet's theorem[3], one can obtain the same solution as before

$$x(s) = \sqrt{\varepsilon}\sqrt{\beta(s)}\,\cos[\Psi(s) + \phi] \tag{17}$$

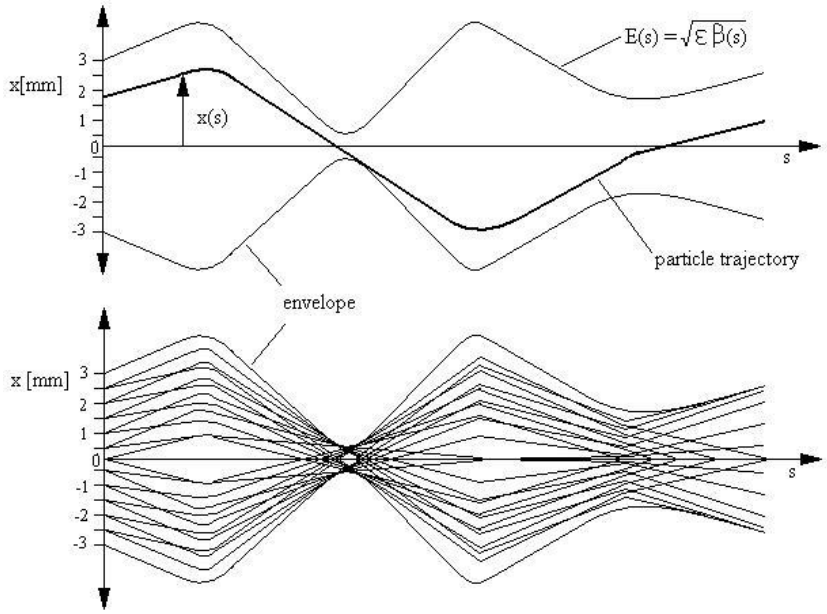

Figure 2.1: Particle trajectories $x(s)$ within the envelope $E(s)$ of the beam. The upper figure shows one single trajectory, while the lower shows 18 different trajectories.

but in this case, the beta function $\beta(s)$ is also periodic. The resonant behaviour depends crucially on the betatron phase $\Delta\Psi = \Psi(s+L) - \Psi(s)$ over one complete revolution. Thus, the **tune** or Q **value** of a circular accelerator is defined as

$$Q \equiv \frac{\Delta\Psi}{2\pi} = \frac{1}{2\pi}\int_0^L \frac{ds}{\beta(s)} = \frac{1}{2\pi}\oint \frac{ds}{\beta(s)}. \tag{18}$$

Due to the periodicity of $\beta(s)$, Q is independent of position s. In simple words, the **tune** represents the number of betatron oscillations a particle undergoes over one complete revolution.

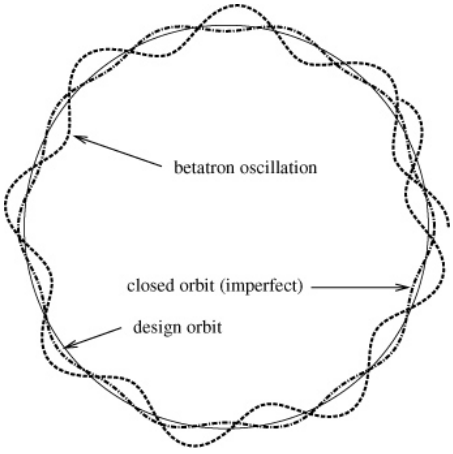

Figure 2.2: Particle trajectories. With the solid line is represented the design orbit, with the dashed line the betatron oscillations and with the dashed-dotted line the closed orbit of the particle.

2.2 Resonances

Perturbation terms in the equation of motion can lead to a special class of beam instability which is called *resonances*. Resonances can occur if perturbations act on a particle in synchronism with its oscillatory motion. The appearance of them is generally restricted only to circular accelerators due to the fact that the perturbations occur periodically at every turn. One can Fourier analyze the perturbation with respect to the revolution frequency and if any of the harmonics of the perturbation terms coincide with the eigenfrequency of the particles, a resonance can occur and the particles may get lost. Resonances caused by field imperfections are called *structural resonances* or *lattice resonances*.

2.2.1 Conditions of Coupling Resonances

In circular accelerators, betatron motion occurs in both the horizontal and vertical plane. Perturbations may be present which depend on the betatron oscillation amplitude in both planes[4]. Such terms are called *coupling terms* and their lowest order term is caused by rotationally misaligned quadrupoles.

Starting from the general equation of motion, as was done before,

$$u''(s) + k(s)u(s) = 0 \tag{19}$$

and by introducing the *Floquet's coordinates* or *normalized coordinates* through the transformation

$$w = \frac{u}{\sqrt{\beta}} \quad and \quad \varphi = \int_0^s \frac{ds}{\nu\beta(s)} \tag{20}$$

one would end up with the following of motion

$$\ddot{w} + \nu_o^2 w = \bar{p}_n(\varphi)\, w^{n-1}. \tag{21}$$

The equation (21) is for the normalized horizontal coordinates for an n^{th} order perturbation in an uncoupled case, while the same applies for the vertical coordinates, too. Since a coupled case is being studied, the same equation of motion for the horizontal plane will be

$$\ddot{w} + \nu_{ox}^2 w = \bar{p}_{nr}(\varphi)\, w^{n-1}\, v^{r-1} \tag{22}$$

where n, r are integers and w, v describe the betatron oscillations in horizontal and vertical plane, respectively and $\bar{p}_{nr}(\varphi)$ represents a general perturbation term. The unperturbed solution of the equation (22) will be of the form

$$w_o(\varphi) = \alpha e^{i\nu_o\varphi} + be^{-i\nu_o\varphi} \tag{23}$$

where α, b are arbitrary constants. The higher order amplitude terms in the perturbation can be expressed by the appropriate sums of trigonometric expressions:

$$\bar{p}_{nr}(\varphi) = \sum_m \bar{p}_{nrm}\, e^{im\varphi}\,, \tag{24}$$

$$w^{n-1}(\varphi) = \sum_{|l|\le n-1} W_l\, e^{il\nu_{ox}\varphi}\,, \tag{25}$$

$$v^{r-1}(\varphi) = \sum_{|q|\le r-1} V_q\, e^{iq\nu_{oy}\varphi} \tag{26}$$

Inserting all the equations above into equation (22) gives

$$\ddot{w} + \nu_{ox}^2 w = \sum \bar{p}_{nrm}\, W_l\, V_q\, e^{i[(m+l\nu_{ox}+q\nu_{oy})\varphi]} \tag{27}$$

where m, l, q are integers. So, the *resonance condition* is

$$m + l\nu_{ox} + q\nu_{oy} = \nu_{ox}. \tag{28}$$

If the same expression for the vertical plane is also derived, they can be written in a more elegant way, as following

$$k\nu_{ox} + l\nu_{oy} = iN \tag{29}$$

or to seem more familiar

$$kQ_x + lQ_y = iN \tag{30}$$

where k, l, i are integers and N is the periodicity of the lattice. The quantity $|l| + |k|$ gives us the order of the *coupling resonance*. For example, for the *PS* the periodicity is 50 and so, if the tunes of a particle satisfy the equation $Q_x + 2Q_y = 50$, it will be on top of the 3^{rd} order resonance $(1, 2)$.

Plotting all straight lines for different values of k, l, i for a specific betatron tune diagram produces what is called a *resonance diagram*. In Fig. 2.3 is presented an example of a resonance diagram for $N = 1$ with resonances up to 3^{rd} order.

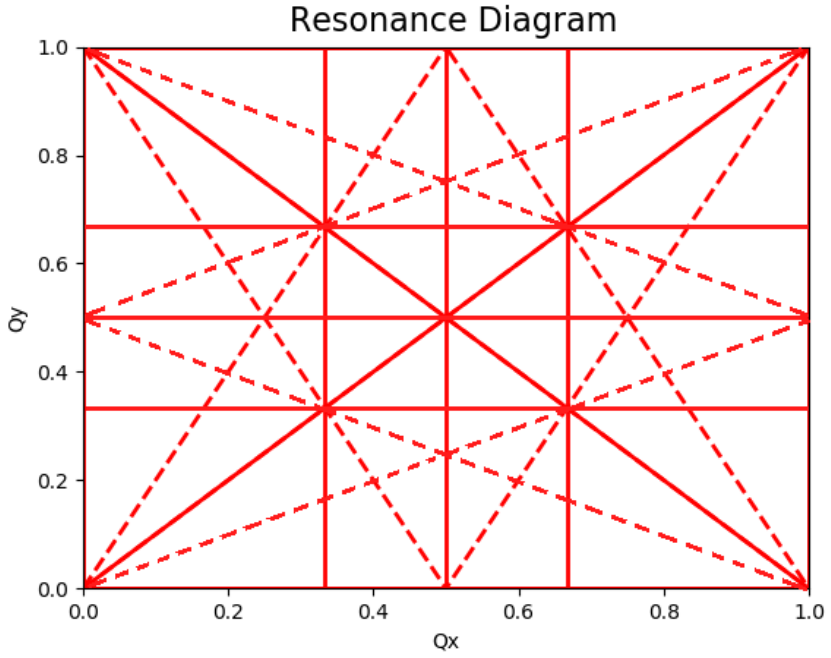

Figure 2.3: Resonance diagram for a ring with periodicity $N = 1$.

In the reality, the resonance lines are not mathematically thin lines but they actually have some thickness, called *stop band width* which depends on the strength of the resonance since not every resonance has the same strength and generally their strength decreases as their order increases.

2.3 Space Charge

In this section, SC will be briefly introduced which is one of most fundamental collective effects in particle accelerators. Its impact is generally proportional to the beam intensity and the main idea is that the charge and current of the beam create self-fields and image fields that alter the dynamic behavior. This influences the single-particle motion as well as coherent oscillations of the beam as a whole.

2.3.1 Direct Space Charge

To begin with, *direct space charge*[5],[6], or the SC that comes from the particles' self-fields, is based on the fundamental electromagnetism of *Coulomb's law* and *Maxwell's equations*. Let's suppose that we have two identical particles with charge $+e$ (Figure 2.4). When these two particles are at rest, they experience a repulsion due to *Coulomb's law*. Though, when they are travelling with velocity $v = \beta c$, they create two parallel currents $I = ve$ which create in turn, a magnetic field making the two particles attract each other. Figure 2.4 shows that the overall effect is still repulsive but as the velocities grow larger, the effect decreases. Also, as special relativity implies, the forces becomes equal at the speed of light and thus, they cancel. That is the reason why *SC* is negligible in larger accelerators as *LHC*, for example.

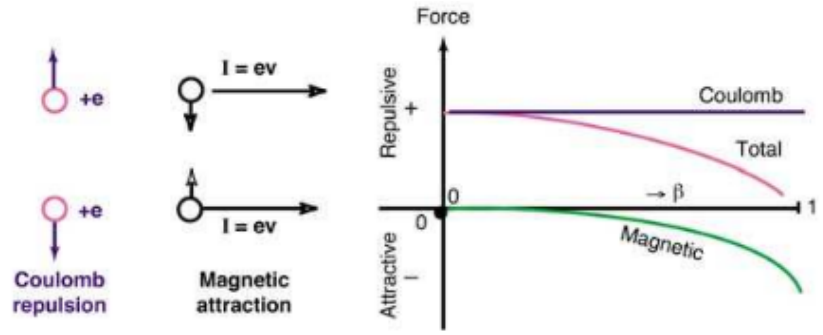

Figure 2.4: Coulomb repulsion and magnetic attraction between two identical particles, at rest and while travelling.

Let an unbunched beam of circular cross section with radius α and uniform charge density $n\,[Cb/m^3]$ be, that moves with velocity $v = \beta c$ that is constant. The line charge density of that beam will be $\lambda = \pi\alpha^2 n\,[Cb/m]$ and its current density will be $J = \beta c n\,[A/m^2]$ with total current $I = \beta c\lambda\,[A]$. Using the cylindrical symmetry and some basic electromagnetism, one can find that the radial electric field of such beam will be

$$E_r = \frac{I}{2\pi\varepsilon_0\beta c}\frac{r}{\alpha^2}. \tag{31}$$

Similarly, the azimuthal magnetic field can be calculated as

$$B_\phi = \frac{I}{2\pi\varepsilon_0 c^2}\frac{r}{\alpha^2}. \tag{32}$$

As one might notice, both the electric and the magnetic fields vanish at $r = 0$ and increase linearly with r up to the edge of the cylinder, $r = a$.

Let a test particle be somewhere inside the beam where it will experience a force due to the fields above. This force will be

$$\overrightarrow{F} = q(\overrightarrow{E} + \overrightarrow{v} \times \overrightarrow{B}) \Rightarrow F_r = \frac{eI}{2\pi\varepsilon_0\beta c}\frac{1}{\gamma^2}\frac{r}{\alpha^2} \tag{33}$$

where $\gamma = 1 - \beta^2$. Expressing this result with the Cartesian transverse coordinates x, y results in

$$F_x = \frac{eI}{2\pi\varepsilon_0 c\beta\gamma^2\alpha^2}x\,, \quad F_y = \frac{eI}{2\pi\varepsilon_0 c\beta\gamma^2\alpha^2}y. \tag{34}$$

SC has a defocussing effect in both planes and if the beam in not uniform, let's say Gaussian, then the effect becomes non-linear.

If some more realistic results are needed, then one has to introduce a non-uniform distribution of the form

$$n(r) = \frac{I}{2\pi\beta c\sigma^2}e^{\frac{-r^2}{2\sigma^2}} \tag{35}$$

where σ denotes the r.m.s. value of the distribution projected on the x or y axis. Following the same procedure as above, the force will be

$$F_r = \frac{eI}{2\pi\varepsilon_0\beta c\gamma^2 r}\big(1 - e^{\frac{-r^2}{2\sigma^2}}\big), \tag{36}$$

which obviously is no longer linear in r. Just to make some future calculations simpler, this result has to be linearized for small r. That would be

$$F_r = \frac{eI}{2\pi\varepsilon_0\beta c\gamma^2}\frac{1}{r}\left(1 - 1 + \frac{r^2}{2\sigma^2} - ...\right) \approx \frac{eI}{2\pi\varepsilon_0\beta c\gamma^2}\frac{r}{2\sigma^2}. \tag{37}$$

2.3.2 Direct *SC*: Incoherent Tune Shift

As was mentioned earlier, direct *SC* leads to defocussing in both planes. Thus, it is expected that particles in high-intensity beams will experience a lowering of their betatron tunes Q by ΔQ.

Starting again with the *Hill's equation* (15) with the addition of a perturbed term $K_{SC}(s)$ that describes the defocussing effect of *SC*, as following

$$x''(s) + \big(K(s) + K_{SC}(s)\big)x = 0, \tag{38}$$

one can derive $K_{SC}(s)$ in terms of the force F_x

$$x''(s) = \frac{d^2x}{ds^2} = \frac{1}{\beta^2c^2}\frac{d^2x}{dt^2} = \frac{1}{\beta^2c^2}\frac{F_x}{m_0\gamma} = \frac{Ir_0}{e\beta^3\gamma^3c\sigma^2}x \tag{39}$$

where $r_0 = e^2/(4\pi\varepsilon_0 m_0 c^2)$ is the classical particle radius and is equal to $1.54 \times 10^{-18}m$ for protons. Also, F_x is the horizontal part of equation (37). So, the *Hill's equation* including *SC* becomes

$$x''(s) + \Big(K(s) - \frac{Ir_0}{e\beta^3\gamma^3c\sigma^2}\Big)x = 0. \tag{40}$$

The incoherent tune shift ΔQ_x that is introduced is readily calculated, for example in [3], by integrating the weighted gradient errors around the circumference $2\pi R$:

$$\Delta Q_x = \frac{1}{4\pi}\int_0^{2\pi R} K_x(s)\beta_x(s)ds = \frac{1}{4\pi}\int_0^{2\pi R} K_{SC}(s)\beta_x(s)ds. \tag{41}$$

Using $K_{SC}(s)$ from equation (40) yields

$$\Delta Q_x = -\frac{r_0 I R}{ec\beta^3\gamma^3}\left\langle \frac{\beta_x}{2\sigma^2} \right\rangle = -\frac{r_0 N}{2\pi\beta^3\gamma^3}\frac{2}{E_x} \; for\, r \ll \sigma \tag{42}$$

with $E_x = 4\sigma^2/\beta_x$, the 95% emittance and $I = Ne\beta c/(2\pi R)$ with N being the number of particles.
As one might notice:

- the tune shift is proportional to the intensity;
- it scales with $1/\gamma^3$, so it is very small for proton enegies beyond $\sim 10\,GeV$ and negligible for electrons;
- it does not depend on the machine radius R.

The **Incoherent motion** refers to the beam as if it consists of many particles, each of which moves inside the beam with its indivicual betaltron amplitude, phase and even tune Q. Amplitude and phase are distributed at random over all particles.

2.3.3 A visual example

In order to visualize the effect of SC on the tunes of a real beam, an example of a *tune diagram*[6] follows.

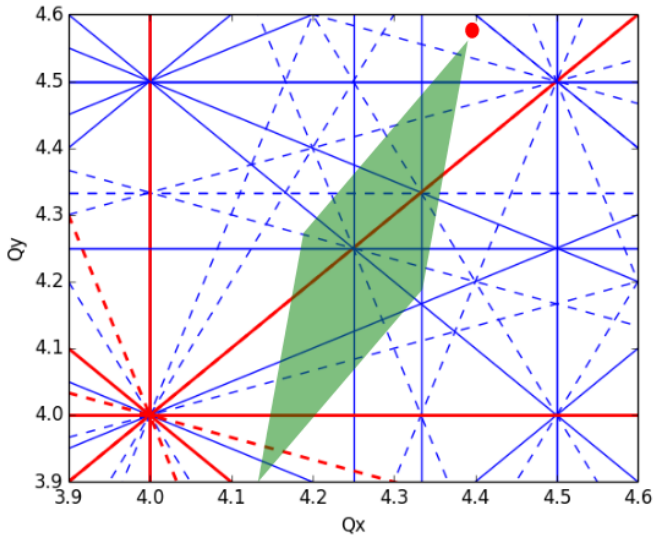

Figure 2.5: Tune Diagram

The red dot represents the WP, namely the tunes that the accelerator is set to work. Due to SC though, the tunes of the particles are shifted and are spread on top of the green diamond which is called *"necktie"*. The closer one particle is to the center of the beam, the larger shift it will experience. As one might notice, the *"necktie"* crosses many resonances and that might lead to many particle losses or beam blow-up.

2.4 Chaos

Chaos comes from the ancient Greece where it referred to the void state preceding the creation of the universe or cosmos in the Greek creation myths. It used to mean vast void, emptiness, abyss, infinite darkness etc. In the modern world, *Chaos* has obtained a quite different meaning which was first seen in Elizabethan Early Modern English. That is the meaning of complete disorder and confusion.

In physics though, *chaos* in used to describe the property of a complex system whose behavior is so unpredictable as to consider it completely random. These kinds of systems show also the property of having great sensitivity to small changes in the initial conditions.

2.4.1 Deterministic Chaos

The term *Deterministic chaos*[7] sounds like oxymoron. One would expect chaotic behavior to stem from randomness since people tend to characterize something that behaves in a very random manner, as chaotic. Though, even something that is random can follow a simple pattern making randomness alone an insufficient condition. In fact, it is not even necessary for a dynamic system to be random in order to be chaotic.

So, what does make a system chaotic? A system is called chaotic when its irregular behavior arises from a strictly deterministic time evolution without any source of noise or external stochasticity. This irregularity manifests itself in an extremely sensitive dependence of the initial conditions which makes impossible to predict the future of the system. Most surprisingly, it turned out that such chaotic behavior can already be found for systems with a very low degree of freedom.

A dynamical system can be described simply as a system of N first-order differential equations

$$\frac{dx_i}{dt} = f_i(x_1, \dots, x_N, r) \ , \quad i = 1, \dots N \ , \tag{43}$$

where the independent variable t can be read as time and the $x_i(t)$ are dynamical quantities whose time dependence is generated by (43), starting from specified initial conditions $x_i(0)$, $i = 1, \dots, N$. It should be noted that the system (43) is autonomous because it is not explicitly t-dependent. The f_i are nonlinear functions of the $x_i$and are characterized by the parameter(s) r. The equations lead to chaotic motion, which develops and changes its characteristics with varying control parameter(s) r. Though, the assumption that the system is autonomous is not necessary since one can convert it to autonomous simply by introducing the time t as an additional variable x_{N+1}.

In this study, the dynamical system are the particles of an accelerator. Sometimes, under some circumstances this systems appears to have chaotic behavior, too. The particles may start all together, very close to each other, but after some time they have completely different orbits and their distance in phase space may have changed dramatically. This might affect the stability of the beam and lead to beam loss, emittance growth, tune shifts, etc. In order to investigate if

there is any chaos there are many tools that one could use such as the *Lyapunov exponent* which will be discussed shortly or, in this case, FMA and CMA.

2.4.2 The Lyapunov Exponent

Chaotic dynamics is characterized by an exponential divergence of initially infinitesimally close points. This divergence is called in mathematics *Lyapunov exponent*. Let's consider the case of one-dimensional discrete maps on an interval

$$x_{n+1} = f(x_n) \ , \quad x \in [0,1] \, , \tag{44}$$

and two orbits starting with infinitesimally different initial conditions x_0 and $x_0 + \Delta x_0$. Their distance after n iterations will be

$$\Delta x_n = |f^n(x_0 + \Delta x_0) - f^n(x_0)| \tag{45}$$

which increases exponentially for **large** n for a chaotic orbit, according to

$$\Delta x_n \approx \Delta x_0 e^{\lambda_L n} \, . \tag{46}$$

One could easily see that

$$\lambda_L = \lim_{n\to\infty} \frac{1}{n} \ln \frac{\Delta x_n}{\Delta x_0} \tag{47}$$

which is the *Lyapunov exponent*. λ_L equals to 1 if there is chaos and 0 when there is just a regular case. In simple words, this exponent "measures" how rapid is the growth of the distance one is interested into. The CMA method uses the *Lyapunov exponent* concept, i.e. it studies the change of distance in phase space as will be shown shortly, but in this project this exponent is not calculated directly due to practical and numerical reasons.

2.5 Frequency Map Analysis [8],[9],[10],[11],[12]

The FMA method was first introduced by *J. Laskar* in order to study the stability of the solar system, as modeled by a reduced 15 degrees of freedom (DOF) system. In this case, frequency analysis made possible to estimate numerically the size of the chaotic zones in all directions of the 15 DOF and revealed that the inner planets (Mercury to Mars) are in large chaotic zones while the outer planets (Jupiter to Neptune) are in much smaller chaotic zones. Nowadays, FMA is widely used in many fields like atomic physics, celestial mechanics, accelerator physics and more.

2.5.1 Frequency analysis

The main idea behind the frequency analysis is the following. Let's suppose that an experiment takes place and data for the position and the momentum of a particle are produced. Thus, there will be the function

$$f(t) = x(t) + ip(t), \tag{48}$$

where $x(t)$ can be any of the DOF of the system. If this function is an integratable, quasi-periodic function, it can be written as

$$f(t) = \sum_{k=1}^{\infty} \alpha_k e^{i\nu_k t} \tag{49}$$

where α_k are of decreasing amplitude with k. The frequency analysis is a numerical method to obtain an approximation

$$f'(t) = \sum_{k=1}^{N} \alpha'_k e^{i\nu'_k t} \tag{50}$$

with a given number of turns N. The frequencies ν'_k and the complex amplitudes α'_k are found with an iterative scheme. In order to calculate the first frequency ν'_1, one have to find the maximum of the amplitude of the function

$$\phi(\sigma) = \langle f(t), e^{i\sigma t} \rangle = \langle f(t), g(t) \rangle, \tag{51}$$

where

$$\langle f(t), g(t) \rangle = \frac{1}{2T} \int_{-T}^{T} f(t)\, \bar{g}(t)\, \chi(t)\, dt \tag{52}$$

with accuracy of determining the main frequencies proportional to $1/T^2$ while an ordinary FFT method has accuracy proportional to $1/T$. By imposing a weight function $\chi(t)$ one can make the method even more accurate. In particular, if one uses the *Hanning window filter*

$$\chi(t) = 1 + cos(\pi t/T)\,, \quad with \ \frac{1}{2T} \int_{-T}^{T} \chi(t)\, dt = 1, \tag{53}$$

can reach accuracy proportional to $1/T^3$. Once the first periodic term $e^{i\nu'_1 t}$ is found, its complex amplitude α'_1 can be obtained by orthogonal projection, and the process is started again on the remaining part of the function

$$f_1(t) = f(t) - \alpha'_1 e^{i\nu'_1 t}. \tag{54}$$

If $f'(t)$ is a good approximation of $f(t)$, a second frequency analysis of $f'(t)$ can be done in order to get its approximation that will be of the form

$$f''(t) = \sum_{k=1}^{N} \alpha''_k e^{i\nu''_k t}. \tag{55}$$

The quantities $\delta\alpha_k = |\alpha''_k - \alpha'_k|$ and $\delta\nu_k = |\nu''_k - \nu'_k|$ give the exact precision of the determination of the amplitudes α'_k and the frequencies ν'_k of $f'(k)$, as obtained by the application of the frequency analysis algorithm. If $f(t)$ is close to $f'(t)$, these same quantities can be considered as estimates on the precision of the determination of the amplitudes a_k and frequencies ν_k of the original function $f(t)$.

2.5.2 Maps creation and Diffusion estimation

By following the procedure that was described in the previous subsection, for many different initial conditions, one can create a frequency map for a specific experiment. There are many tools that automate the procedure of tune evaluation, like NAFF and SUSSIX. The latter will be briefly discussed later.

Another feature of the FMA is the diffusion of the frequencies. The diffusion coefficient can be calculated via the integral (52) with shifted by t limits $(t, t+T)$ and find the frequency, let's say ν_t. Thus, the diffusion coefficient will be

$$D = \log(|\nu_t - \nu|), \tag{56}$$

where ν is the first frequency that was calculated in Eq. (52) for $(0, T)$. In this project though, the microscopic diffusion is evaluated and the equation that is mentioned above would be more useful in the following form

$$D = \log \sqrt{(Q_x^1 - Q_x^2)^2 + (Q_y^1 - Q_y^2)^2}, \tag{57}$$

where the exponents denote each of the twin particles. In FMA, the stable regions and the non-linear or chaotic regions, can be easily distinguished. The larger the diffusion coefficient is, the larger tune shift will experience the specific particle and so, the larger the chaotic region that it is inside (Fig. 2.6). The whole set of particles creates what we call the *'footprint'*.

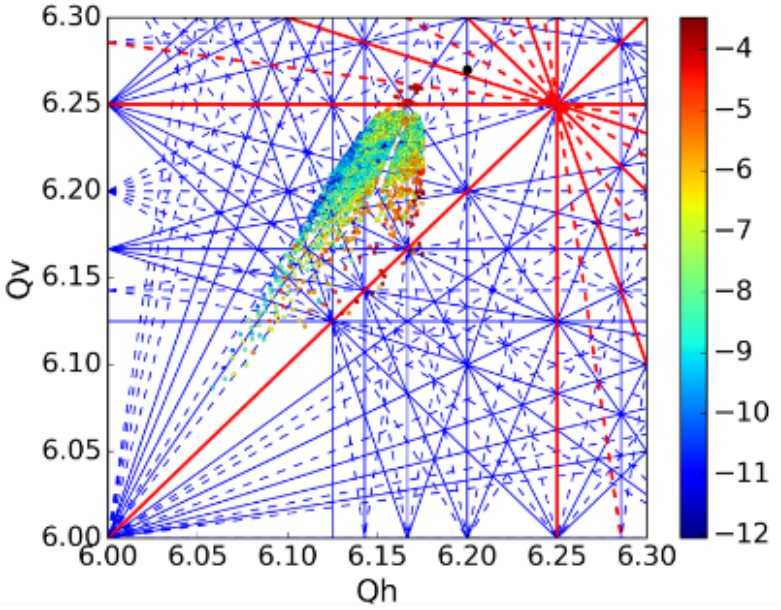

Figure 2.6: Tune Diagram created with the frequency map analysis method. The black dot stands for the WP, while the rest dots are the tunes for different initial conditions. The color bar indicates the diffusion rate. The red color, indicates high diffusion regions or chaotic regions while blue color indicates lower diffusion regions or stable regions.

3 CMA Tool - Description

The development of the *Chaos Map Analysis* (CMA) method is based on the results of a PS Experiment[13] joined by GSI and CERN that took place in 2012. In this experiment the purpose was to study the interplay between SC and a coupled 3^{rd} order resonance. To do that, the tune working point (WP) had to be chosen that it would be well-separated from other excited resonances. One sextupole has been excited to drive the resonance $(1, 2)$ in a Q_x WP regime of $6.04 - 6.25$ while the vertical tune is kept constant at 6.47. It was found that the emittance blow-up becomes large close to this resonance (see Fig. 3.1).

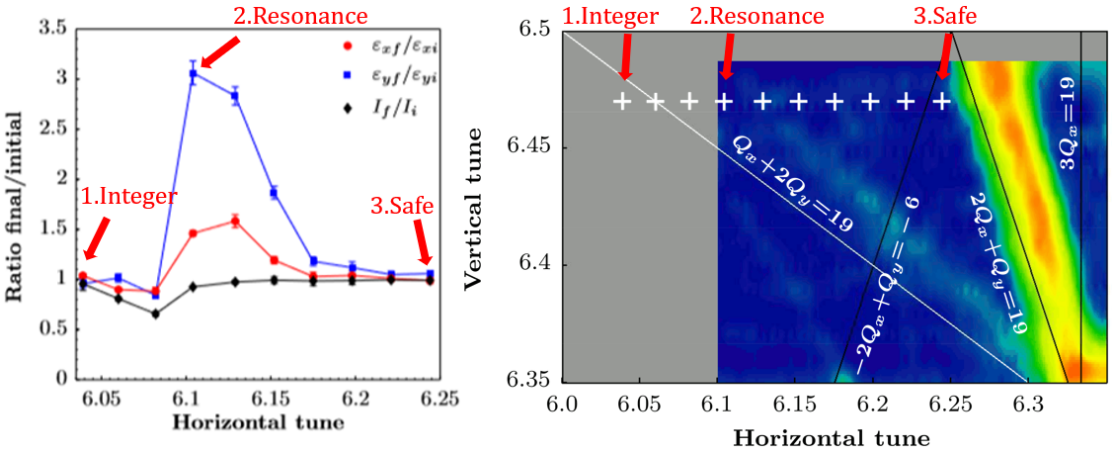

Figure 3.1: Emittance blow-up due to a coupled resonance in combination with SC. The 3 working points that will be studied are indicated. The key words in red will be explained in the text.

Three WPs of the experiment were chosen, as indicated in Figure (3.1), for the development and testing of the CMA technique. These 3 WPs represent 3 interesting and quite different cases. The first WP is a tricky case since it is close to the integer. The second WP is of great interest since it is crossing the resonance $(1, 2)$ being excited by the sextupole, as was in the experiment. Last, the third WP should be very stable since there are no excited resonances nearby. In this way we sample a very wide regime of parameters required for starting a new technique.

The feature of the CMA is to run the simulations with the same a distribution of one thousand particles as in the simulations for the experiment, plus two test particles but to save only the two test particles' data in order to minimize the storage requirements. Depending on the evolution of the test particles' phase space one can conclude if the specific case is regular, weakly chaotic or strongly chaotic as will be shown in subsection (3.3.4). By combining all different cases, one can create maps which are expected to be comparable with the ones made with FMA. A more detailed view of the WPs and the CMA method in general, will be discussed shortly in the sections that follow.

3.1 Tools

A various number of tools had to be used for the simulations and the data analysis. The first one and maybe the most important one is *MAD-X* with which all the simulations were done. *MAD-X* is the 10^{th} version of *MAD* which was developed at CERN and is a general-purpose tool for charged-particle optics design and studies in alternating-gradient accelerators and beam lines. This tool is able to handle from medium to very large machines like LHC and solves various problems on such machines. More information about *MAD-X* and how it is used, can be found in [14].

The second most important tool that was used in this project is *SUSSIX*. Based on the FORTRAN programming language, *SUSSIX* has been developed to post-process tracking or experimental data via frequency analysis. This tool allows to evaluate relevant dynamical quantities such as detuning, betatron tunes, resonance driving terms and smear directly from the recorded turn–by–turn data. In this case, it was of great help in evaluating accurately the betatron tunes in order to make the maps for the CMA and FMA. More information about *SUSSIX* can be found in [15].

Besides those two important tools, many other codes were developed in order to carry through with this project. The amount of different cases and data was enormous, so some codes to automate the analysis were made. Another code was created in order to scan all the data determine if there is chaos in any specific case. In addition, some other codes were created to gather up all the usable data and write them into files so that they can be plotted. All these codes were in FORTRAN, and LINUX's *bash scripts* and *cshell scripts*.

3.2 CMA Parameters

As was explained in the Introduction (Section 1) CMA had to be applied for many different parameters to create a 6D grid. As was shown in the beginning of the Section (3), the CMA technique is applied to three different tunes: one that is close to the integer, one that is crossing the $(1, 2)$ resonance and one that is considered "safe". The three tunes are the following:

1. *Safe Tune* : $Q_x = 6.244$, $Q_y = 6.465$
2. *Resonance Tune* : $Q_x = 6.104$, $Q_y = 6.476$
3. *Integer Tune* : $Q_x = 6.039$, $Q_y = 6.479$

Typically for a frequency map are required many particles, sometimes of the order of ten or hundred thousands, in order to create a footprint. In the CMA case though, it is possible to have much more less particles. To accomplish that, a *"grid"* is created, with different initial conditions of the two test particles.

As far as the transverse coordinates are concerned, five different angles of emittance ratios were chosen. The five angles are the following

- $\phi = 15°$,
- $\phi = 30°$,
- $\phi = 45°$,
- $\phi = 60°$,
- $\phi = 75°$.

Also for each angle, there were chosen 20 different emittance amplitudes with equal distance between them ($\sim 0.5\sigma$). For any amplitude that is located on top of an arc as is indicated in figure 3.2, applies that $\varepsilon_x + \varepsilon_y = constant$.

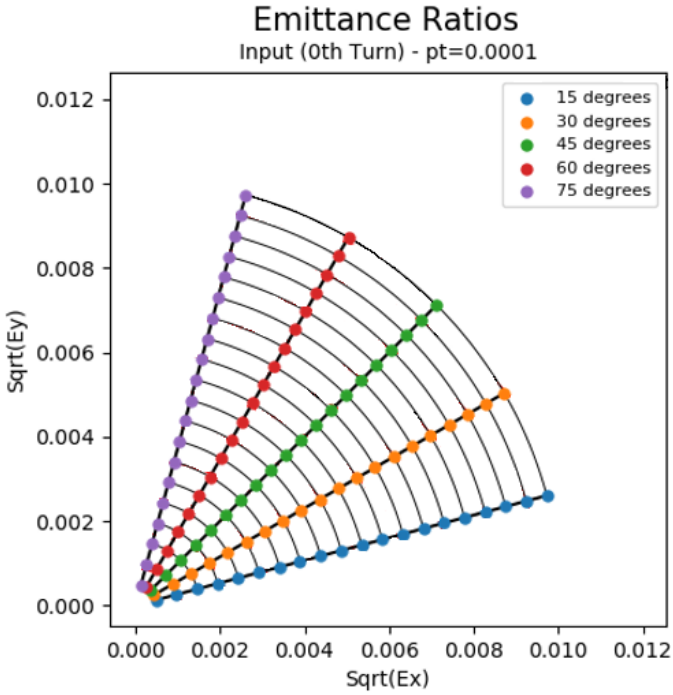

Figure 3.2: Emittance Rations for five different angles.

As far as the longitudinal coordinate is concerned, the parameter that is easier to be controlled is the P_t which is a MAD-X canonical variable and is defined as

$$P_t = \frac{\Delta E}{p_0 c}, \quad where\ \Delta E = \frac{E - E_0}{E_0}. \tag{58}$$

P_t stands for the position of the particle in the longitudinal distribution. The greater the P_t is, the more away our particle is from the center of the distribution. For these simulations, 3 different P_t values were used which are the following

$$P_t = 1.980 \times 10^{-5} \sim 0.02\sigma_l,$$
$$P_t = 0.975 \times 10^{-3} \sim 1\sigma_l,$$
$$P_t = 1.950 \times 10^{-3} \sim 2\sigma_l.$$

For each P_t value there will be a different footprint. For the smallest P_t value which can be considered to be for the "on-momentum" particles since its value is very small and the motion is mainly transversely, the footprint is expected to be on a perfect grid as shown in figure (3.3). For the rest 2 values, the footprint will be smaller due to the weaker SC force as one moves out of the distribution.

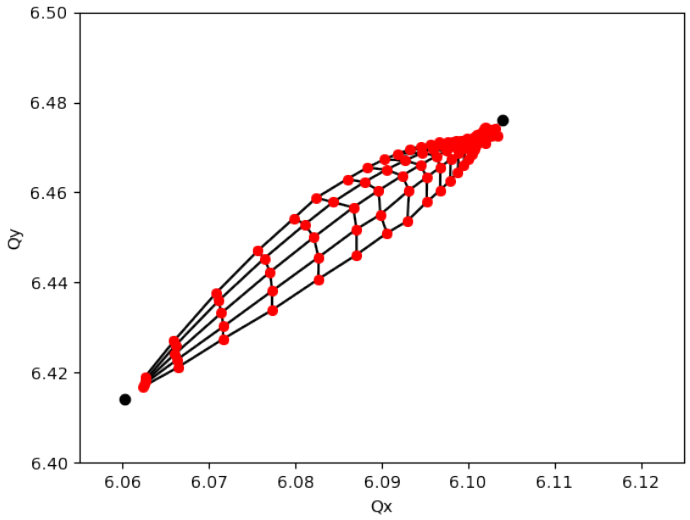

Figure 3.3: Grid of Particles for $0.02\sigma_l$.

This is how the 6-Dimensional phase space was fully parametrized and this will help examine how the particles behave depending on their location around the beam distribution for every combination of the parameters mentioned above.

Last but not least, the CMA technique is applied to two lattices both of which will be shown later. The first one is a very simple toy lattice (Section 5) and the PS lattice (Section 6).

3.3 CMA Technique

In this chapter, the whole procedure that took place in the CMA technique will be described. It will be divided into four brief subsections. The first one will be the setting up of the simulations, the second one will be the description of the data analysis, the third one will be an explanation of the angular distance of the particles and the forth one will be the procedure that was followed in order to characterize all of the cases.

3.3.1 Simulation Set-up

In this study there was a great number of different simulations. As was discussed in subsection (3.2), for each machine there were 3 tunes following with 3 different P_t values and for each P_t value, 5 angles times 20 amplitudes. All these numbers sum up to 1800 different simulations which needed a specific procedure to be set up and when done, analyze their data to get the desired results.

The first thing to be done was to create the lattice input file. In order to use the lattice of each machine, some arrangements needed to be done first. Some parameters, for example the beam intensity was kept constant. Though, the lattice input file had to be optimized for each different tune, since the quadrupole strengths need to change.

Additionally, a particle distribution needs to be created. To do that, a simple Gaussian distribution was produced that was matched to each tune. In addition, on top of the distribution two test particles were added arbitrarily with the amplitudes that are shown in figure (3.2) for each P_t value. Furthermore, these data was in normalized coordinates so they had to be converted to laboratory's coordinates of a specific lattice, by using a FORTRAN code that was provided.

After everything was set up, a MAD-X code was used in order to call all the files and do the tracking correctly. This code simulated the behaviour of the distribution for 12000 turns in the machine which corresponds to $8 - 10$ synchrotron periods. Most of the cases were done in MAD-X's *adaptive mode* in which the emittance of the beam is updated in every turn in order to change the SC kick. Though, as will be discussed in the text, some cases had to be done in MAD-X's *frozen mode*, too. This mode keeps the SC kick "frozen".

3.3.2 Data Analysis

After all simulations were done, the tracking data had to be analyzed to produce some results. First of all, the data had to be normalized back again to have less "noise" in the frequency analysis. After that was done, SUSSIX was used to evaluate the *synchrotron tune* and afterwards to calculate the *betatron tunes*. The betatron tunes were calculated for most of the cases for 8 full *synchrotron periods*. For some specific reasons, as will be shown in the next section (Section 4) the tunes had to be calculated in some cases for various number of synchrotron periods. Also, in that section it will become obvious why it was chosen to calculate the tunes for 8 periods and not for any other smaller number of periods.

In order to do the FMA plots with the diffusion, the procedure that was described in chapter (2.5) has to be followed. That is, calculating the diffusion **between the 2 test particles** since they both start from the same point with infinitesimal difference. For the CMA though, a quite different procedure has to be followed. With a FORTRAN code, the data was analyzed so as to create a file that has only the *angular distance* of the phase space of the two particles with respect to the turns inside the machine. As will be shown shortly , depending on the behavior of the *angular distance* one can conclude if there is chaos or not (Section 3.3.4). By combining all these results, it is feasible to create the chaos maps.

3.3.3 Angular Distance in Phase Space

In order to understand better the angular distance that is studied to conclude if a case is chaotic or not, an example will be presented. Let's suppose that there are two test particles which are simulated for N turns around the machine with their position in phase spaces (see Fig. 3.4) analyzed. In the horizontal phase space plane there is phase difference or angular difference φ_x between the two particles, in the vertical plane φ_y and in the longitudinal plane typically the difference is insignificant.

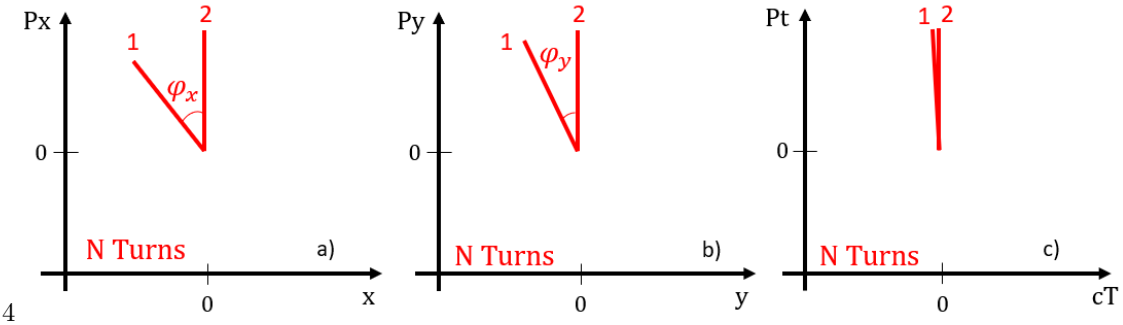

4

Figure 3.4: Angular distance between two particles after N turns. a)Horizontal plane, b)Vertical plane, c)Longitudinal plane.

Subsequently, if these two particles do another N turns, there will be 3 different cases.

First, there is the case of the regular motion (see Fig. 3.5). In this case the two test particles after $2N$ turns end up with twice the angular distance values that they had for N turns, namely $2\varphi_x$, $2\varphi_y$ while φ_t is still negligible. So the angular distance grows or decreases **linearly** and consequently the motion of the two particles is **regular**.

The next relevant case is concerned with **weakly chaotic** motion (see Fig. 3.6). In this case the angular distances are not exactly twice the initial values but they are a somewhat larger. That means that the change starts to exhibit weakly chaotic motion non compatible with regular behaviour or most likely weakly chaotic motion. However, it might also very well be that over a very long time scale the motion actually remains regular. In fact, the chaotic nature can only be "proven" once it actually exhibits strong chaotic behaviour (see next paragraph).

Last, if the angular distances of the particles after $2N$ turns are much larger than the ones that they had for N turns (see Fig.3.7), they exhibit **strongly chaotic** motion. The property of this motion is that the angular distance change in a rapid, non-regular way. In fact the motion is unpredictable or strongly chaotic in a deterministic manner.

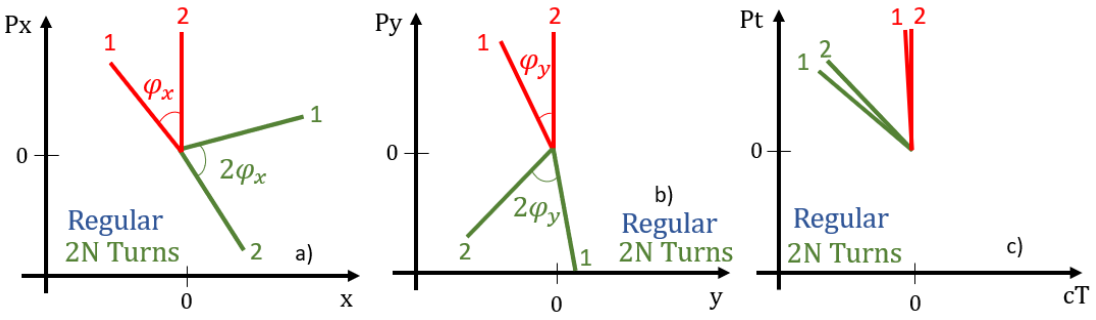

Figure 3.5: Angular distance between two particles after 2N turns - Regular Case. a)Horizontal plane, b)Vertical plane, c)Longitudinal plane.

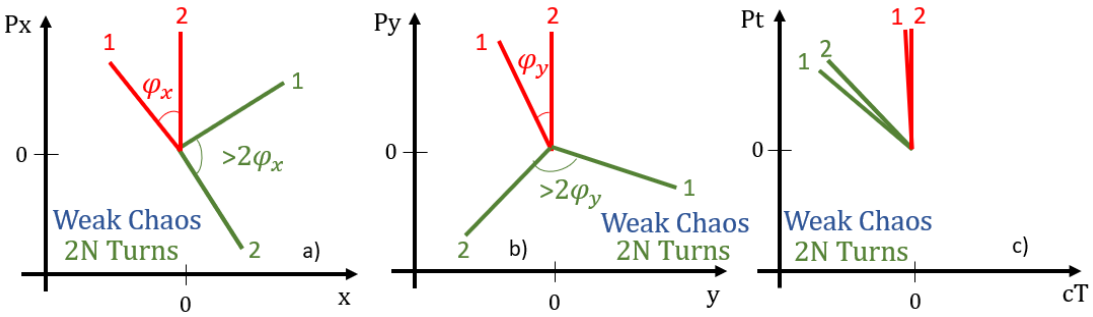

Figure 3.6: Angular distance between two particles after 2N turns - Weakly Chaotic Case. a)Horizontal plane, b)Vertical plane, c)Longitudinal plane.

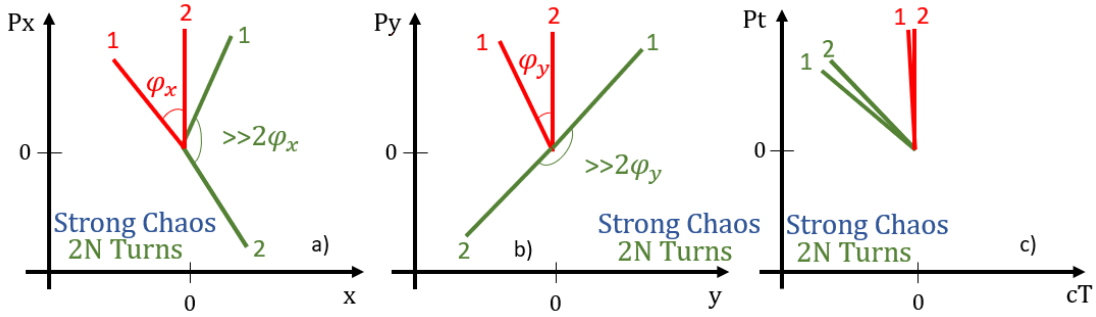

Figure 3.7: Angular distance between two particles after 2N turns - Strongly Chaotic Case. a)Horizontal plane, b)Vertical plane, c)Longitudinal plane.

3.3.4 Chaos Characterization

Particles can exhibit three different kinds of motion. The phase spaces of a particle for each of these motions are shown in Figure (3.8). The longitudinal phase space is not presented since for all three cases seems similar.

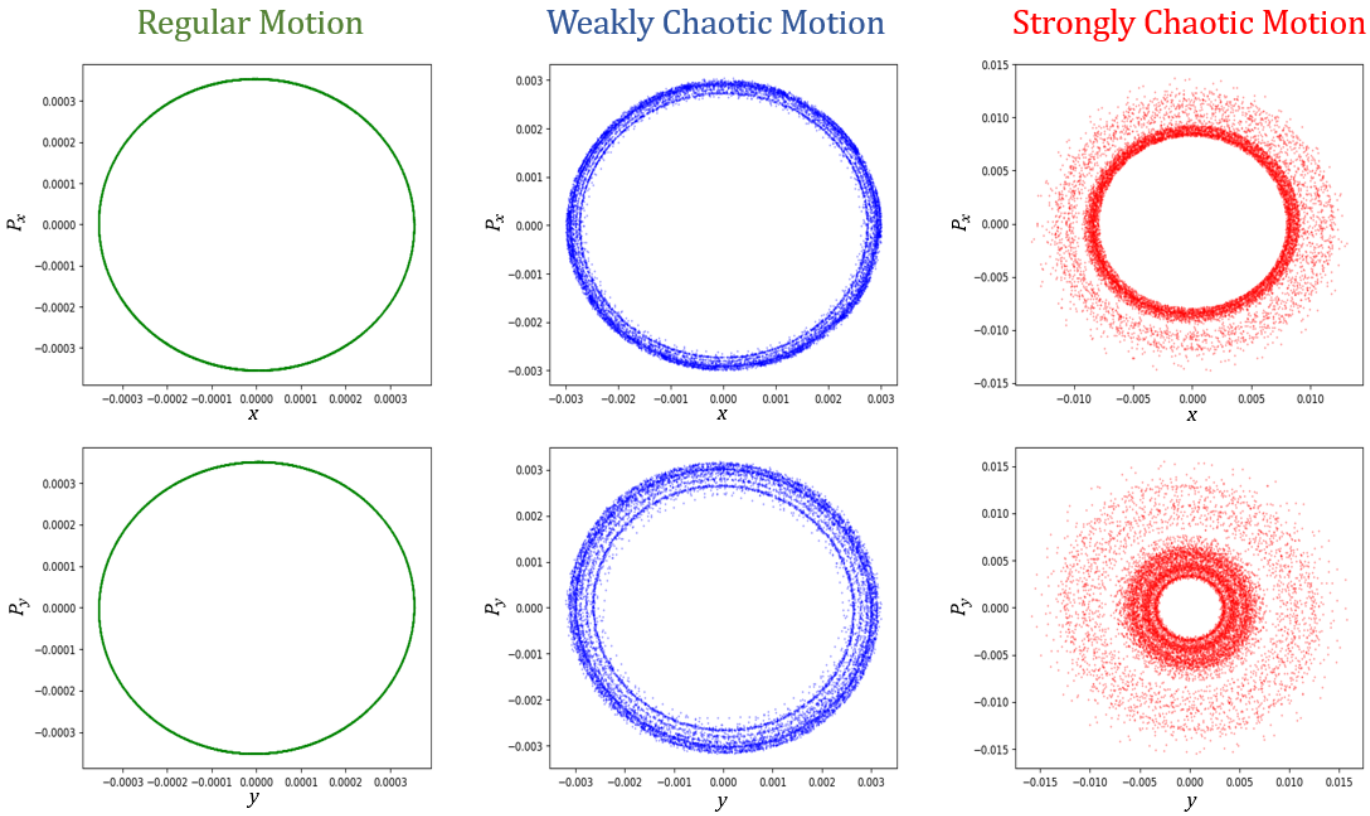

Figure 3.8: Transverse phase spaces of Regular, Weakly Chaotic and Strongly Chaotic motions.

Regular motion means that particles oscillate in the transverse planes without any significant amplitude or momentum change. In phase space, this corresponds to a perfect circle as indicated in the figure. When the particle is located in a weakly chaotic region, its oscillations are not stable resulting in a small amplitude change. Only after a large number of turns, that amplitude change becomes noticeable and that is the main reason why the two aforementioned cases are difficult to be distinguished at an early stage. The strongly chaotic motion results in a rapid amplitude growth. The oscillation in phase space is no more well defined as was in the regular motion, and the width of the ring can cover large areas for a small number of turns as indicated in the last set of diagrams.

Defining an algorithm to identify these three cases is not obvious and in some cases can be an arduous procedure. There are many methods of identifying the kind of motion like evaluating the r.m.s. action from the phase spaces. In this study a different approach was chosen to conclude the nature of motion. In general, the amplitudes of the transverse oscillations evolve very slowly, as shown in [16]. On the contrary, angular distance evolves much faster making it suitable for

early chaos detection providing also great sensitivity, even for weak chaos. To this end, it was chosen to study the angular distance of the twin particles.

A FORTRAN code was used to evaluate the angular distance of the twin particles for each turn (see Fig. 3.9). These figures indicate the **total** angular distance for all 3 planes and for all 3 kinds of motion that was described in the last section. Note that the max angular distance of each plane is normalized so as if we add all 3 together to sum up to 1.

The linear growth of the angular distance (Fig. 3.9.a) corresponds to the **regular** case. When the angular distance starts to grow in a non-linear manner, the motion becomes **weakly chaotic** ((Fig. 3.9.b). Last, when the angular distance grows or decreases exponentially with an unpredictable behaviour, then the motion is **strongly chaotic** (Fig. 3.9.c).

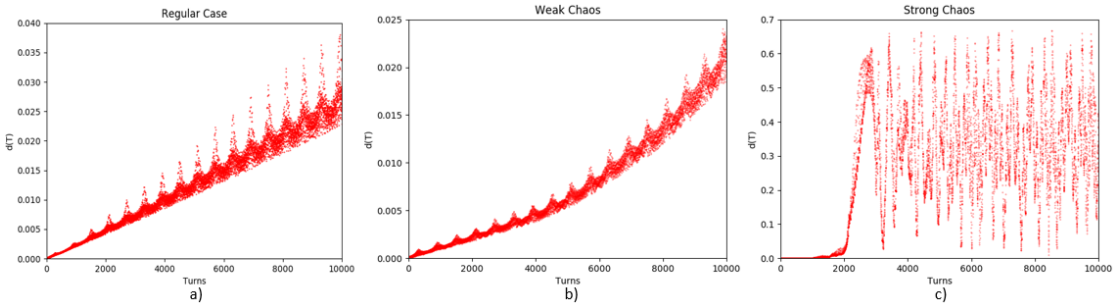

Figure 3.9: Angular distance - Turns diagrams. a)Regular motion, b)Weakly chaotic motion, c)Strongly chaotic motion.

Another benefit of using this procedure is that the development of a code that distinguishes the motion of particles, is simpler. This code uses some criteria that have been chosen to make it possible to determine in which case particles are into without having to look each angular distance plot separately.

The easiest case to distinguish is the **strongly chaotic** case. If the total angular distance, reaches values over 0.5 then it is strong chaos and it will have red color in the chaos plots. Technically, this means that the twin particles reach maximum angular distance to at least 2 of the 3 planes.

The regular and weakly chaotic cases are difficult to be distinguished and so they are studied together. It is needed to plot the angular distance in terms of turns on a double-logarithmic-scale plot and evaluate the slope for different number of synchrotron periods, e.g. slope for the 1^{st} synchrotron period, then for the first 2 periods, then for the first 3 periods. Plotting the slopes in terms of the synchrotron periods denotes the motion that the particle is into.

When these slopes converge to 1 (see Fig. 3.10) means that the angular distance grows or decreases linearly and particles exhibit a **regular** case. In the CMA plots, green color stands for regular cases.

If these slopes do not converge to 1 but they increase or decrease, then it will be a **weakly chaotic** case. In the CMA plots, the weakly chaotic cases will be presented with a variety of

colors between green and red depending on their strength. The strength is determined from the average value of the angular distance over the 8^{th} synchrotron period of the data.

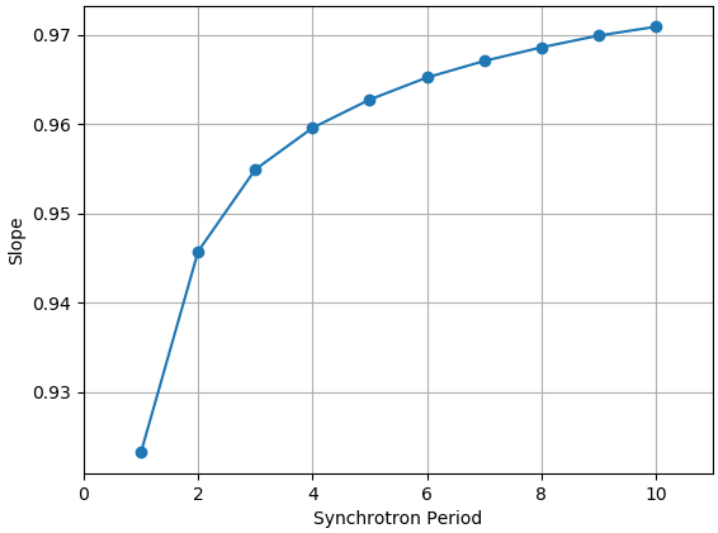

Figure 3.10: Converging slopes for each synchrotron period - Regular Case.

4 CMA - Benchmarking

The CMA technique is based on the ability to detect even weakly chaotic motion. It is well-known[1],[17] that a minimum number of turns is required to find the true nature of particle motion. Additionally, there is the restriction of determining tunes over full synchrotron periods. Moreover, it is desirable to restrict the simulations to the lowest number of synchrotron periods, to minimize the simulation effort.

This can be seen as a benchmarking procedure of the CMA technique to determine after which number of synchrotron oscillations a convergence of the onset of chaos can be reached. The benchmarking procedure goes as follows: apply the CMA technique to an increasing number of synchrotron periods until convergence has been reached. To this end, the tunes and the chaos strength were evaluated first for 1 synchrotron period, then for 2, then for 3, etc. In addition, it is necessary to do the same thing for the FMA to have a comparison.

First, a problem with the CMA method had to be solved. As was mentioned in section (3.3.4), to characterize a case as regular or weakly chaotic, a number of different slopes is needed, to see if they converge or not. For small number of synchrotron periods, it was required to split the synchrotron periods to smaller, sub-periods. In that way, there are more slope values in order to apply the usual method. By nature this can only be an approximation since very reliable results can only be gained from full synchrotron periods.

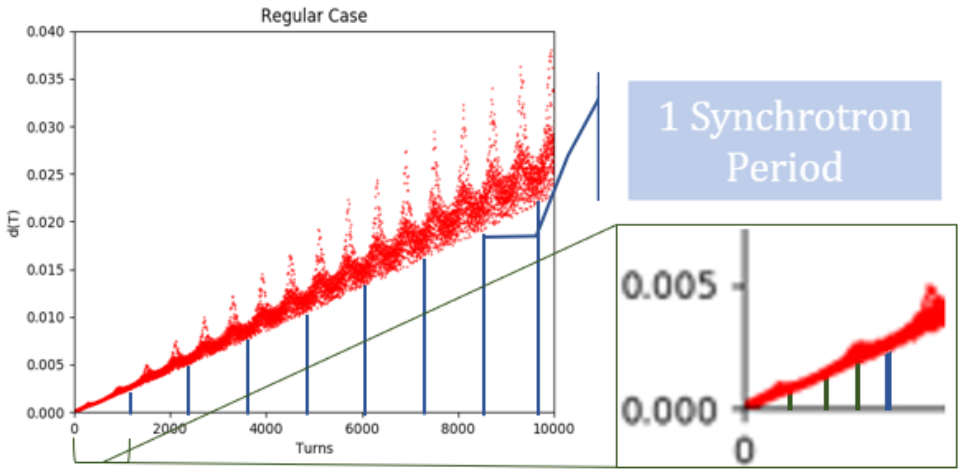

Figure 4.1: Synchrotron sub-periods.

The full results of the benchmarking can be summed in the following table.

Synchrotron period number	Strongly chaotic particle number	Strongly chaotic particle ratio
1	0	0%
2	2	8%
3	11	42%
4	15	58%
5	19	73%
6	21	81%
7	25	96%
8	26	100%

Increasing the number of synchrotron periods, the number of chaotic particles increases, too. Though, for large number of synchrotron periods there is a convergence in the number of strongly chaotic particles, especially from 7 synctrotron periods to 8 synchrotron periods there is only one strongly chaotic particle more. Supposing that the most reliable result is for 8 synchrotron periods, the third column of the table can be evaluated. The strongly chaotic particle ratio stands for the reliability of the results for each number of synchrotron periods.

Thus, as was mentioned in the section (3.3.2), it was decided to apply the CMA method for 8 synchrotron periods since the number of chaotic particles gets saturated after 7 periods and the data was enough for 8 periods. Therefore, all the results that are going to be presented from now on, will be for 8 synchrotron periods. All the results results of the benchmarking can be found in the *Appendix A*. Additionally, in *Appendix A* can be found a walk through for all the plots that are going to follow, as well.

5 Toy Model

It is prudent to test the CMA technique on a simple machine before applying it to a real, complex one. Therefore, a *toy lattice* had to be created which does not possess any non-linearities that would affect the beam.

In particular, the toy lattice is similar to PS in terms of its length ($L = 625\,m$) and its periodicity ($P = 50$). The significant difference is that the toy consists of 50 identical *FODO cells*. That type of cell is one of the simplest ones. It consists of a focusing quadrupole, a defocussing quadrupole and drift spaces between them. Additionally, a sextupole was added in one of these cells to drive the resonance that is mentioned in Section (3).

The initial emittance-amplitude-grid that was used is similar to the one that was mentioned earlier (see Fig. 5.1). The difference in this specific case is that the 1^{st} amplitude of each angle refrains from the 2^{nd} one $\sim 0.25\sigma$ instead of 0.5σ. The amplitudes are sampled to $\sim 15\sigma$ on the vertical plane and 12σ on the horizontal plane. In most of the cases the important part of the beam distribution is up to roughly 8σ.

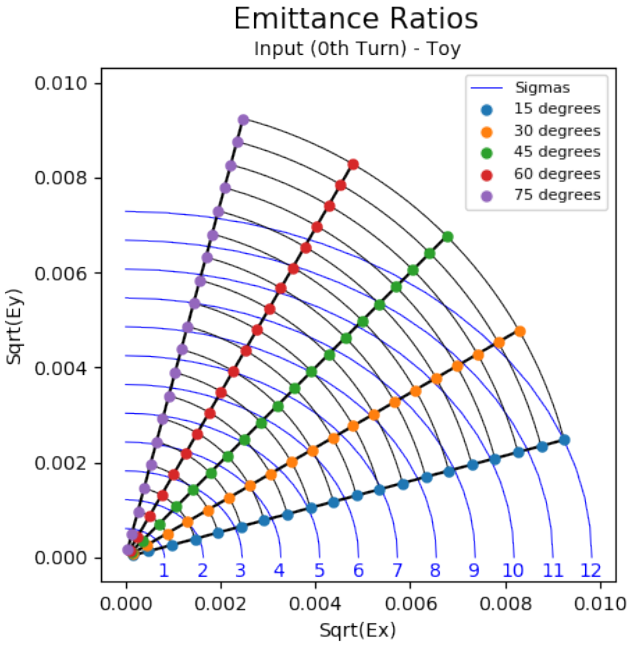

Figure 5.1: Initial emittance amplitudes - Toy

5.1 Resonance Tune

For the toy lattice, only the *Resonance Tune* case will be presented to see the effect that the resonance $(1, 2)$ has on the beam. As was mentioned in the section (3.2), the tunes are $Q_x = 6.104$, $Q_y = 6.476$ for the 3 P_t values $0.02\sigma_l$, $1\sigma_l$ and $2\sigma_l$.

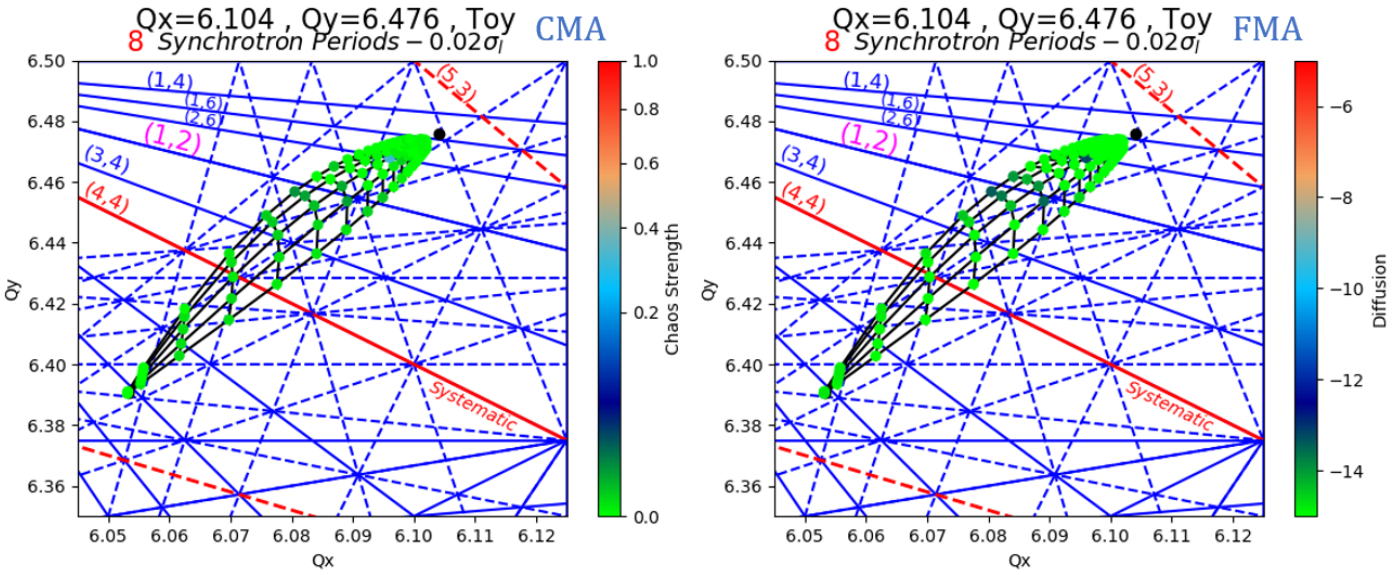

Figure 5.2: CMA and FMA footprints for $0.02\sigma_l$.

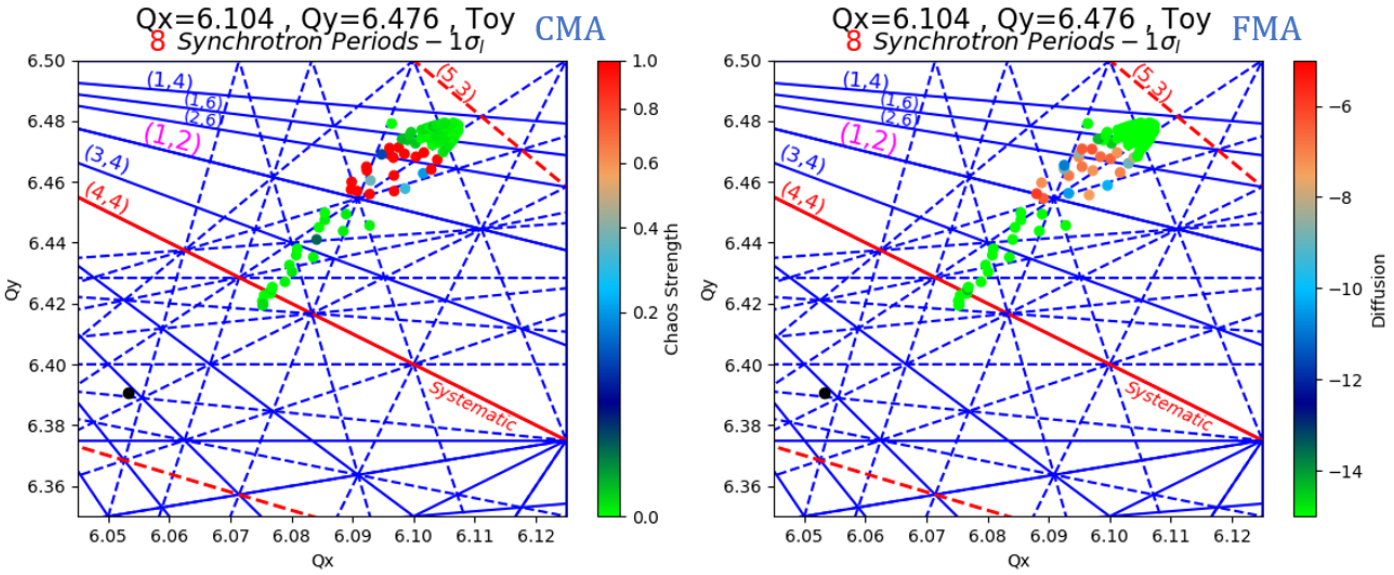

Figure 5.3: CMA and FMA footprints for $1\sigma_l$.

For the on-momentum case particles are expected to be mostly in regular motion (see Fig. 5.2). In this case, there is no synchrotron motion and the resonance does not have a significant impact on the particles. There are only some weakly chaotic particles around it. Both CMA and FMA seem to agree with each other.

For higher longitudinal sigmas due to synchrotron motion, the resonance starts to affect the particles (see Fig. 5.3). Around the excited resonance appears a strongly chaotic region in the CMA case and the same region with high diffusion in the FMA case. The rest particles appear to be mostly regular. Note that for larger longitudinal sigmas, the footprint becomes smaller due to the weaker SC force.

When the edge of the longitudinal distribution is studied, particles appear to be mostly in regular and weakly chaotic motion (see Fig. 5.4). Some individual particles appear to be strongly chaotic, too. Most of the particles are gathered in a small area due to the weak SC force, so it is difficult to distinguish each particle. The very few cases that are away from this area are possibly due to numerical errors during the tune evaluation.

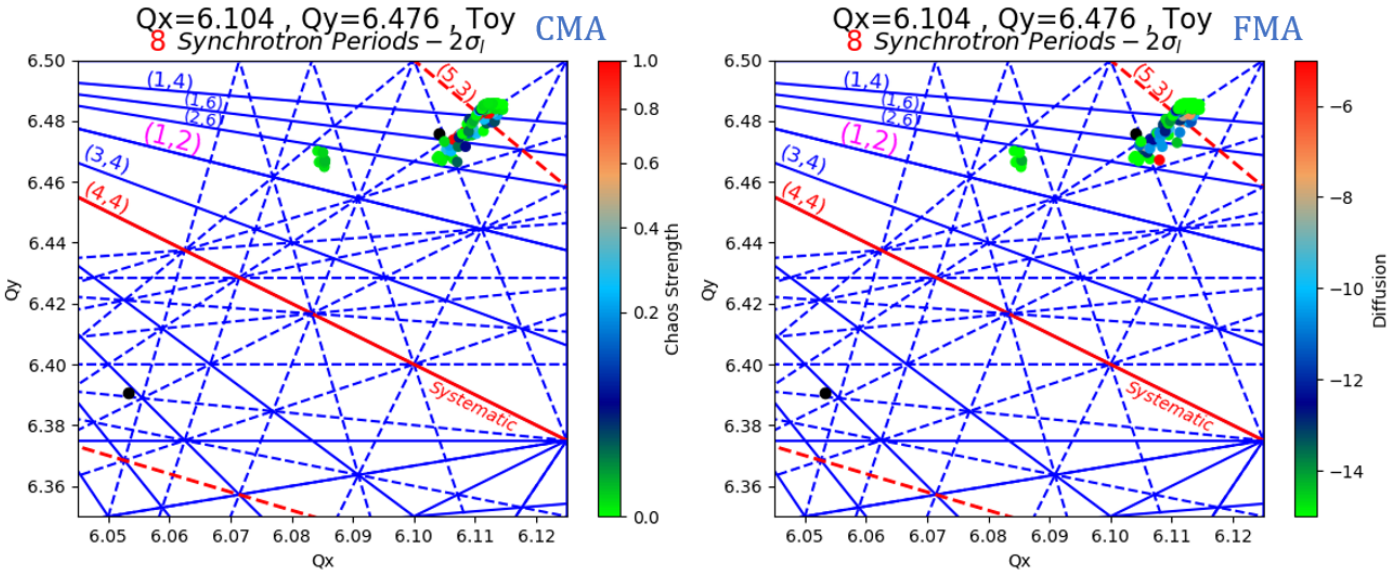

Figure 5.4: CMA and FMA footprints for $2\sigma_l$.

In the toy model, both methods agree in a surprisingly level. Therefore, the CMA technique works for simple lattices and produces reasonable results. Thus, the CMA technique is rippe to be applied on a more realistic machine.

6 PS

The main subject of study of this thesis is the PS machine. In this section will be presented the results of the CMA technique for this particular lattice. The main difference between the PS and the toy lattice is that PS uses combined function magnets. The exact lattice can be found online.

For this case, all three tunes mentioned in Section (3.2) will be presented. Note that, again, there is a sextupole turned on in order to study the effects of the 3^{rd} order resonance $(1, 2)$ in combination with SC. PS might have some imperfections in contrast to the toy, e.g. field errors, misaligned elements etc. Thus, there is a possibility of other excited resonances, too.

The initial emittance-amplitude-grid for this case, is the same as the one presented in Section (3.2) (see Fig. 6.1). The sigmas of the distribution for this case are different due to the different beta functions of the lattice. For both planes, the first amplitude for every angle is $\sim 0.5\sigma$. On the horizontal plane the 20^{th} amplitude reaches $\sim 9.5\sigma$ while on the vertical plane $\sim 11.5\sigma$.

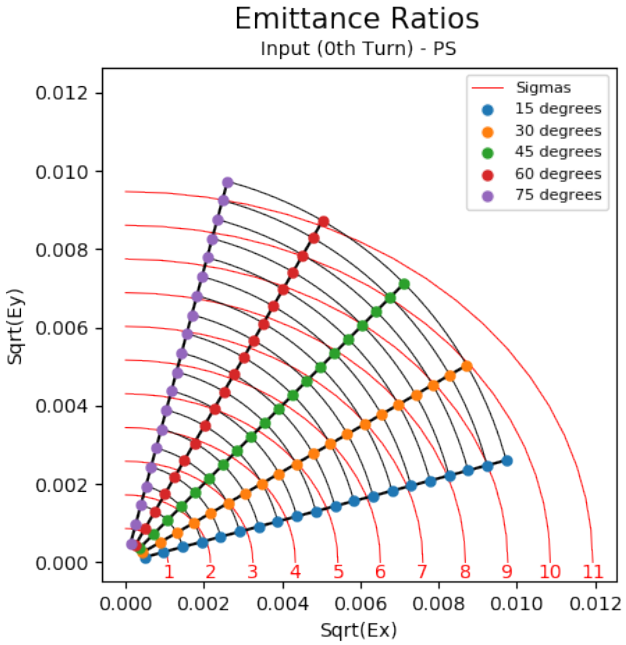

Figure 6.1: Initial emittance amplitudes - PS

The results for the PS lattice will be presented in the forthcoming sections, starting with the *Safe tune*, being the simplest one.

6.1 Safe Tune

The name of this particular case indicates that is the most regular case of the three. This WP is away from any dangerous resonance and so, it is not expected to see any significant chaotic behavior, as will be shown shortly. This was the first case that was studied in PS due to its simplicity and its predictable results.

Particles in the center of the beam exhibit regular motion (see Fig. 6.2). Though, there are some weakly chaotic cases, especially on the resonances $(1, 6)$ and $(2, 4)$. Even at the limit of the beam center or the $1\sigma_l$ of the longitudinal distribution, particles are in regular motion with the exception of some weakly chaotic ones (see Fig. 6.3).

At the edge of the longitudinal particle distribution there is a large synchrotron motion activity. In some cases that might affect the particles' sensitivity to resonances. Though, for the safe tune, particles seem stable (see Fig. 6.4). Only some particles located on the strong systematic resonance $(8, 0)$ have chaotic behaviour or large diffusion in the FMA case. For all three sigmas of the longitudinal distribution, both CMA and FMA seem to agree.

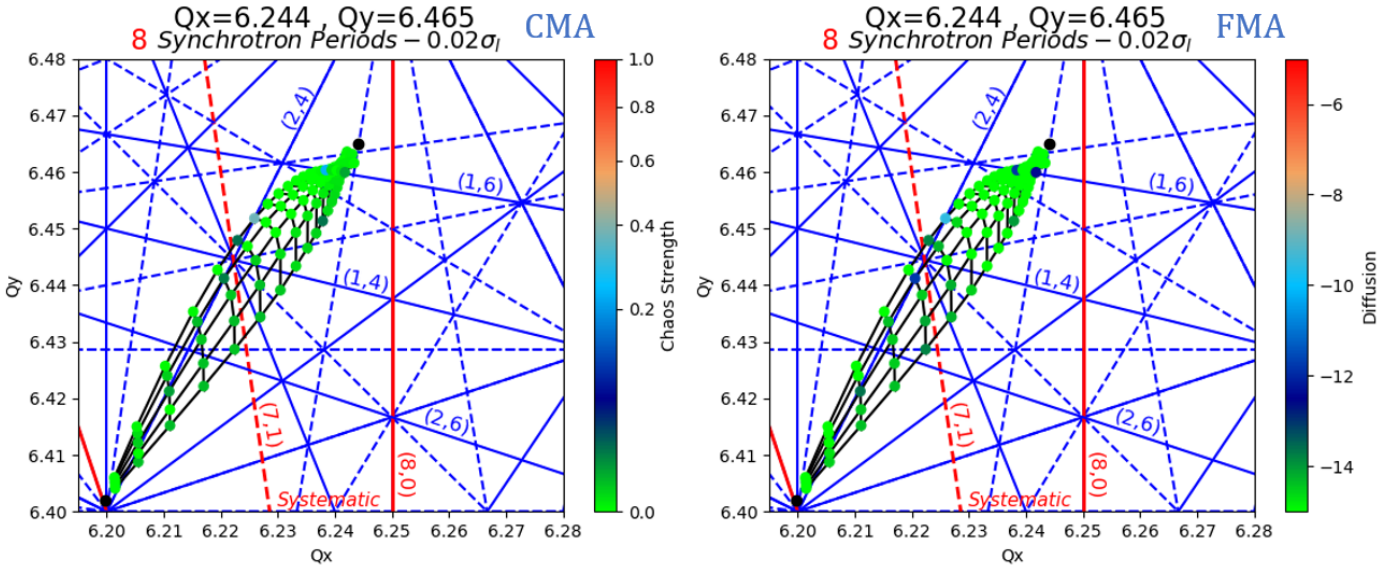

Figure 6.2: CMA and FMA footprints for $0.02\sigma_l$ - Safe tune.

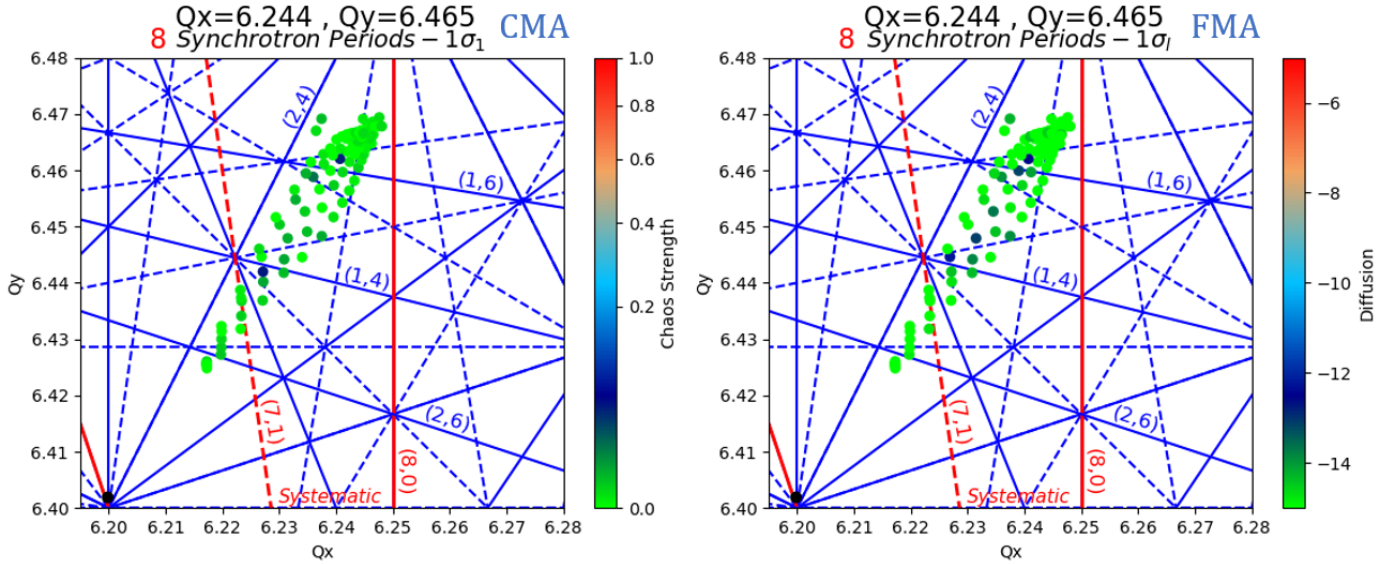

Figure 6.3: CMA and FMA footprints for $1\sigma_l$ - Safe tune.

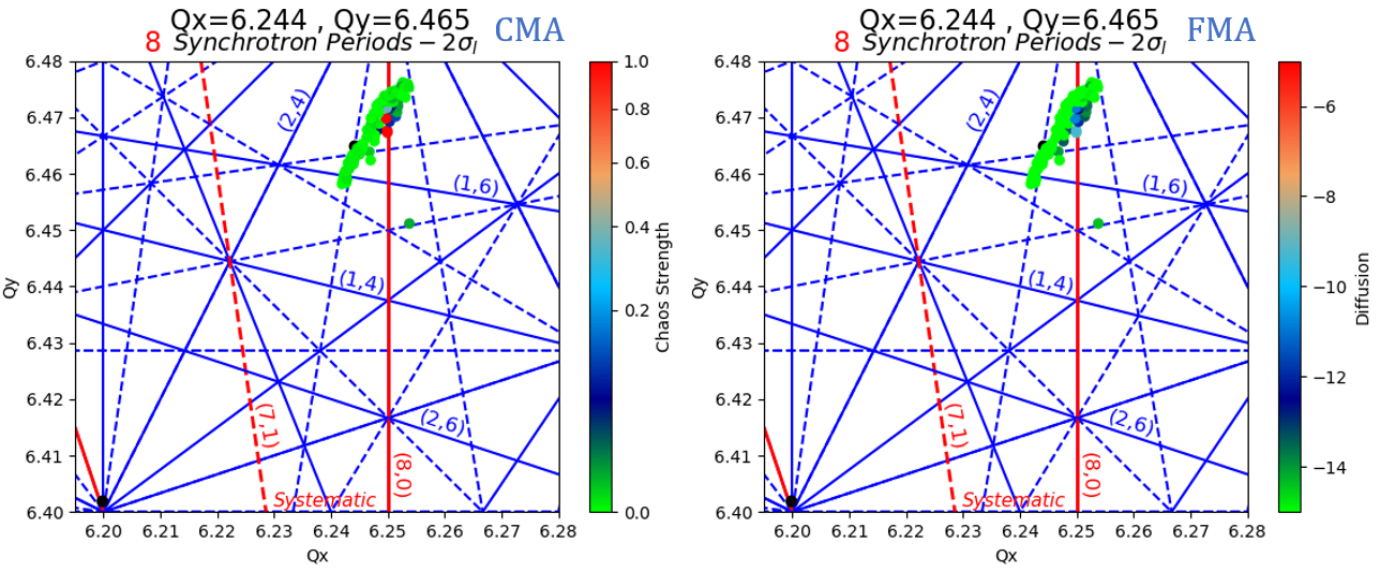

Figure 6.4: CMA and FMA footprints for $2\sigma_l$ - Safe tune.

6.2 Resonance Tune

The *resonance tune* was maybe the most interesting case and the one that needed the most attention. Due to SC tune spread, particles cross the $(1, 2)$ resonance which is driven by a sextupole. This results in the creation of a chaotic region close to this resonance. Additionally, this case had an interesting particularity which will be discussed in the text.

The on-momentum particles whose motion is mainly transverse, exhibit regular motion as in the safe tune (see Fig. 6.5). Similarly, there are some very weakly chaotic particles, too. In the $1\sigma_l$ case though, the synchrotron motion starts to have an impact on the particles (see Fig. 6.6). Close to the excited resonance $(1, 2)$ a region is created where all particles have strongly chaotic motion. There are also chaotic particles above this resonance which might be due to other resonances or the shrinking of the footprint as time passes by.

At the edge of the longitudinal distribution where particles experience less tune spread, particles that are found close to the systematic skew resonance $(5, 3)$ exhibit strongly chaotic motion (see Fig. 6.7). The rest particles appear to be mostly weakly chaotic. In all three cases, the two methods seems to be in agreement.

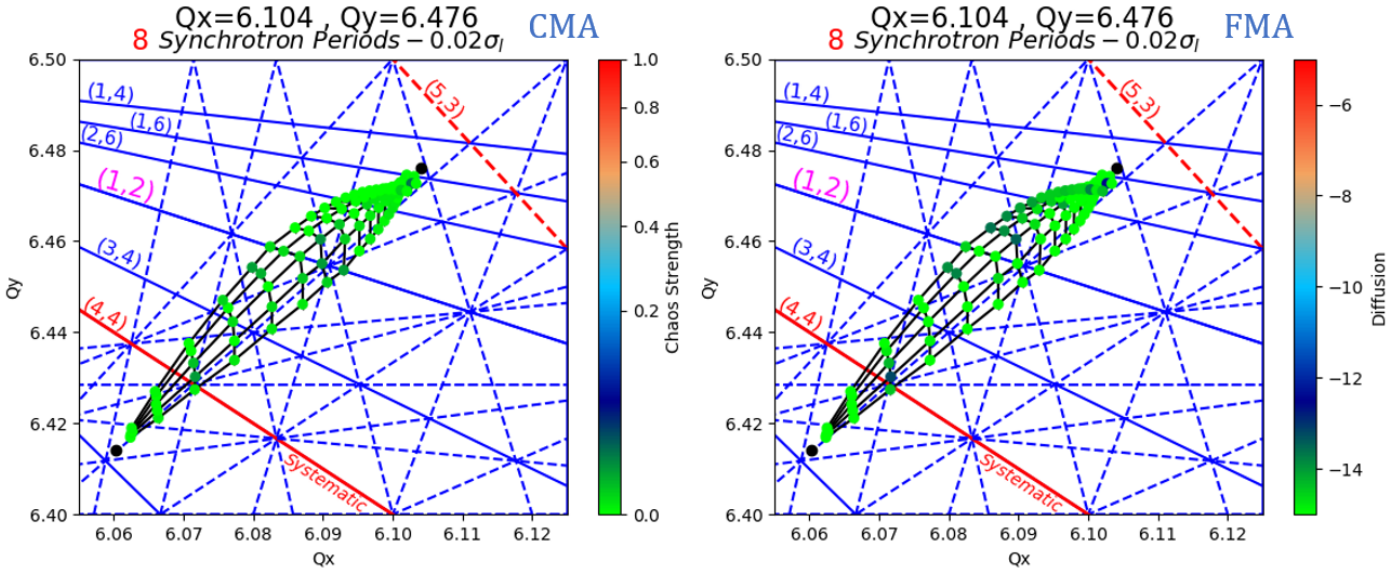

Figure 6.5: CMA and FMA footprints for $0.02\sigma_l$ - Resonance tune.

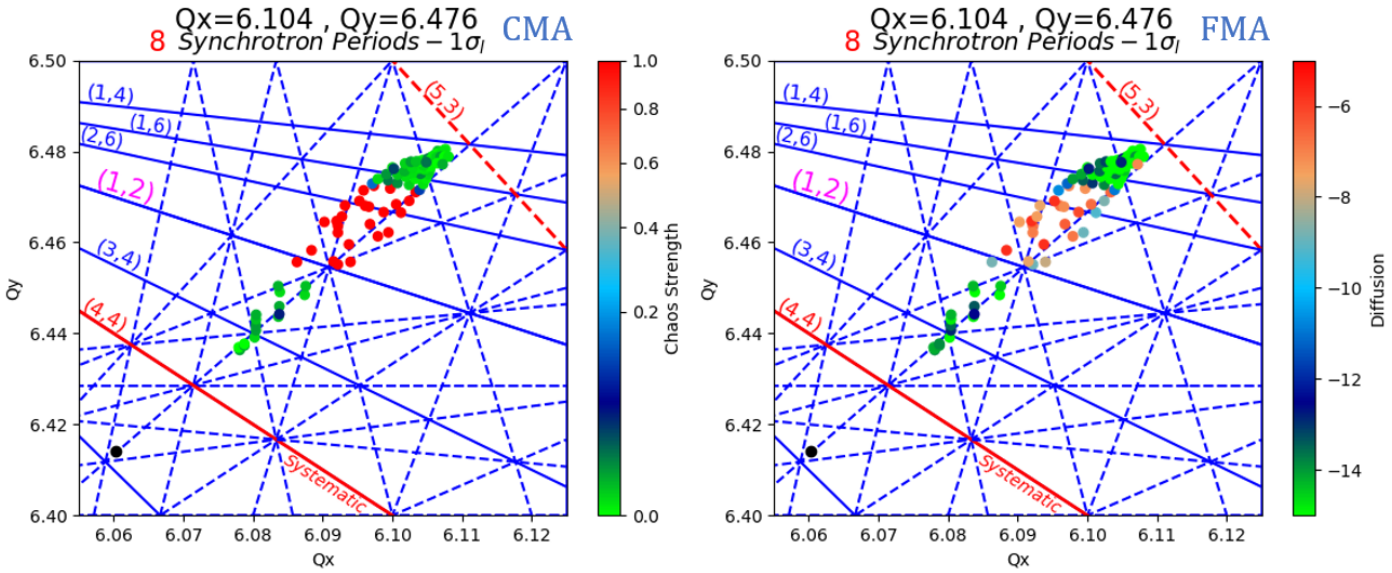

Figure 6.6: CMA and FMA footprints for $1\sigma_l$ - Resonance tune.

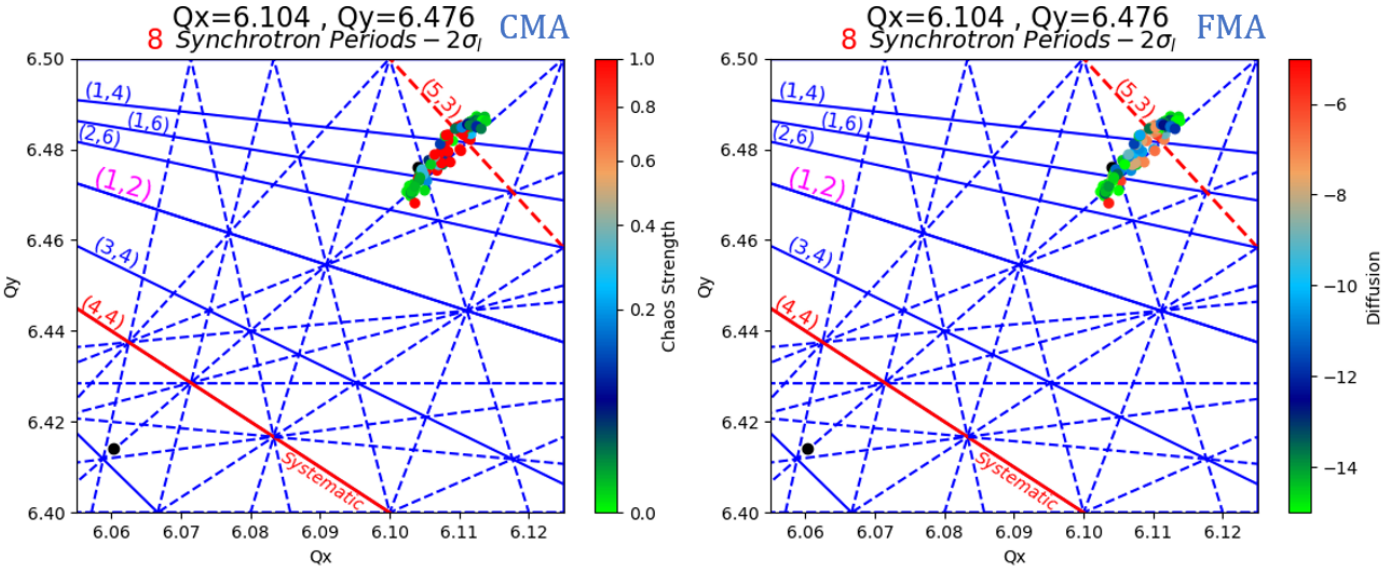

Figure 6.7: CMA and FMA footprints for $2\sigma_l$ - Resonance tune.

During the analysis of these results, which are in MAD-X's *adaptive mode*, something peculiar was noticed. In general, the FMA method was done with two ways. The presented results are done by evaluating the diffusion between the twin particles while the other way it done by evaluating the diffusion of a single particle over four synchrotron periods. In this particular case,

a large diffusion of the on-momentum particles was encountered and had to be examined (see Fig. 6.8).

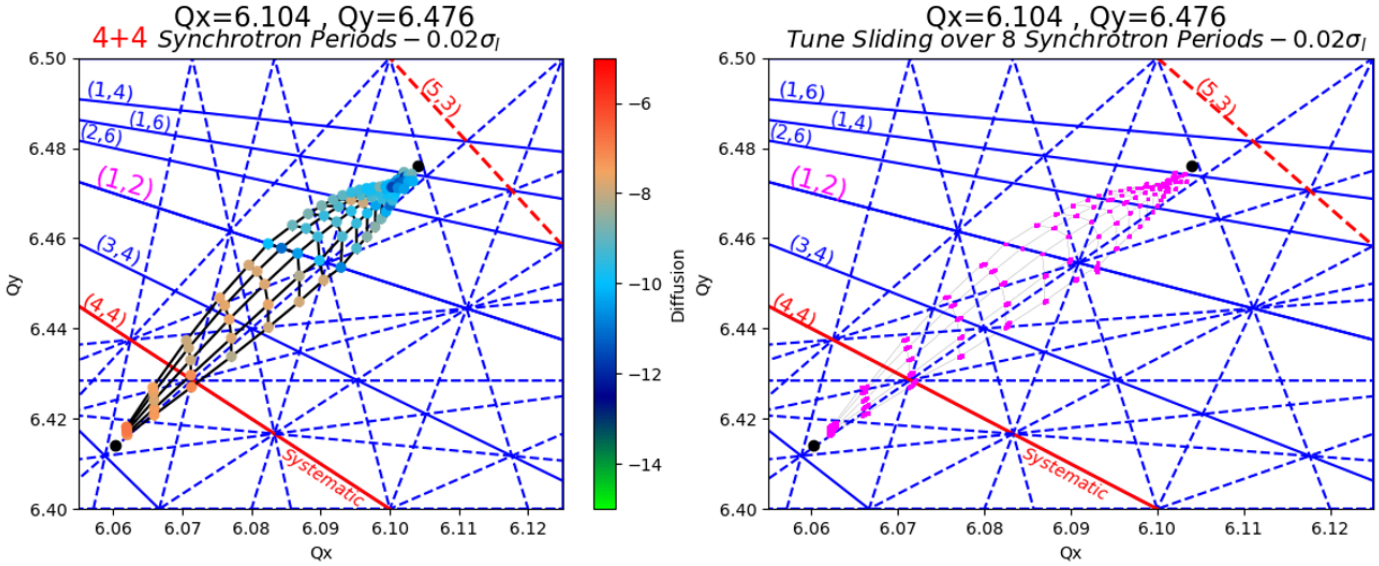

Figure 6.8: Different approach of FMA and tune sliding for $0.02\sigma_l$ - Resonance tune - Adaptive mode.

Evaluating the tunes of a single particle for a range or turns $(0+i, \frac{1}{Q_s}+i)$ where $i = 0, 1, ..., \frac{7}{Q_s}-1, \frac{7}{Q_s})$ can create a *tune sliding* plot (see Fig. 6.8) which shows how the tune of the particle moves over 8 synchrotron periods. This plot confirms that the tunes of the particles of the low amplitudes diffuse. A MAD-X's *frozen mode* study was done to see if this diffusion persists.

6.2.1 Frozen Mode

Simulating this case with MAD-X's *Frozen Mode* showed that the diffusion of the low amplitude particles has diminished (see Fig. 6.9). The only diffusion that was noticed was on some resonances, as expected.

The results that were produced with the CMA and the usual FMA method show that the behaviour of the particles is almost the same as with the MAD-X's *adaptive mode*. For the center of the beam most particles are in regular motion with a new strongly chaotic particle on the resonance $(2, 6)$ (see Fig. 6.10).

At the $1\sigma_l$ of the longitudinal particle distribution the same strongly chaotic region close to the excite 3^{rd} order resonace is encountered (see Fig. 6.11).

At the edge of the longitudinal distribution $(2\sigma_l)$, particles are found with the same behaviour as in the *adaptive mode* (see Fig. 6.12).

In conclusion, the study of the *frozen mode* showed that even though the diffusion of a single particle is mended, the results when studying both particles do not change significantly.

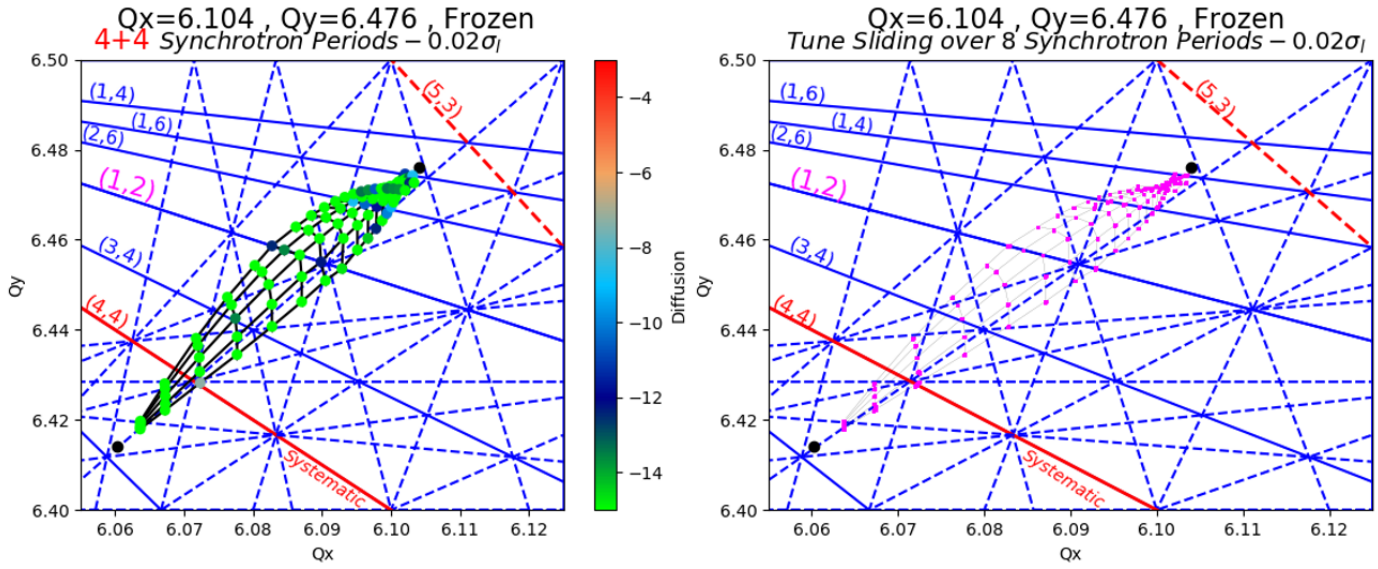

Figure 6.9: Different approach of FMA and Tune sliding for $0.02\sigma_l$ - Resonance tune - Frozen mode.

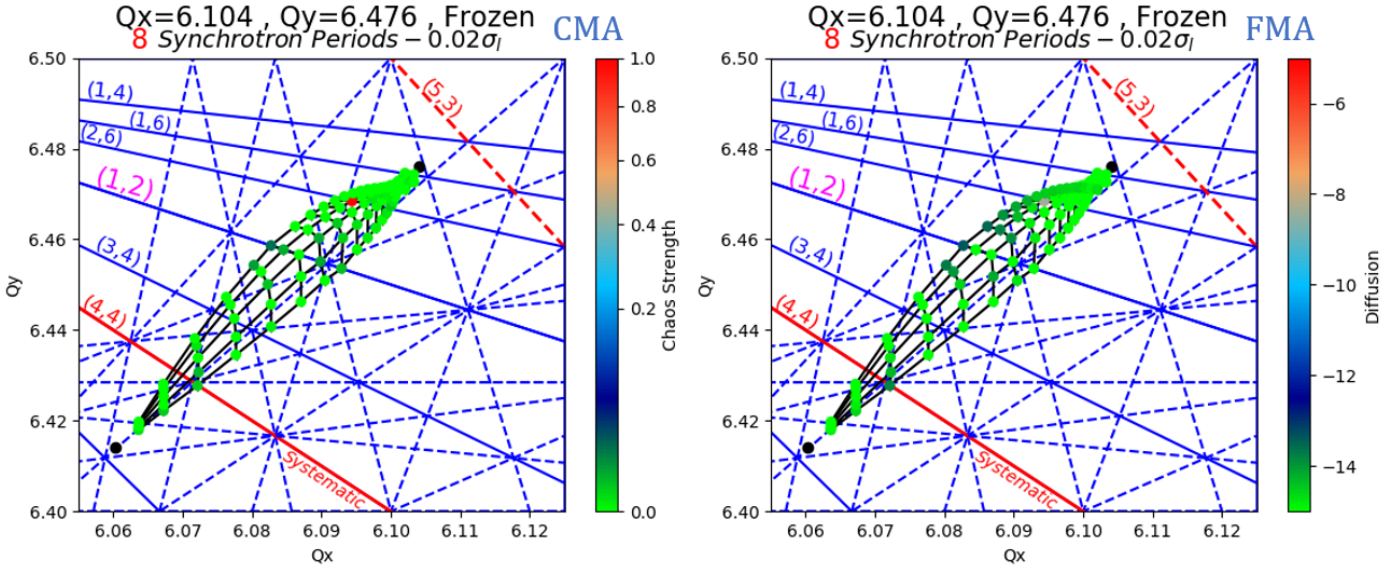

Figure 6.10: CMA and FMA footprints for $0.02\sigma_l$ - Frozen mode - Resonance tune.

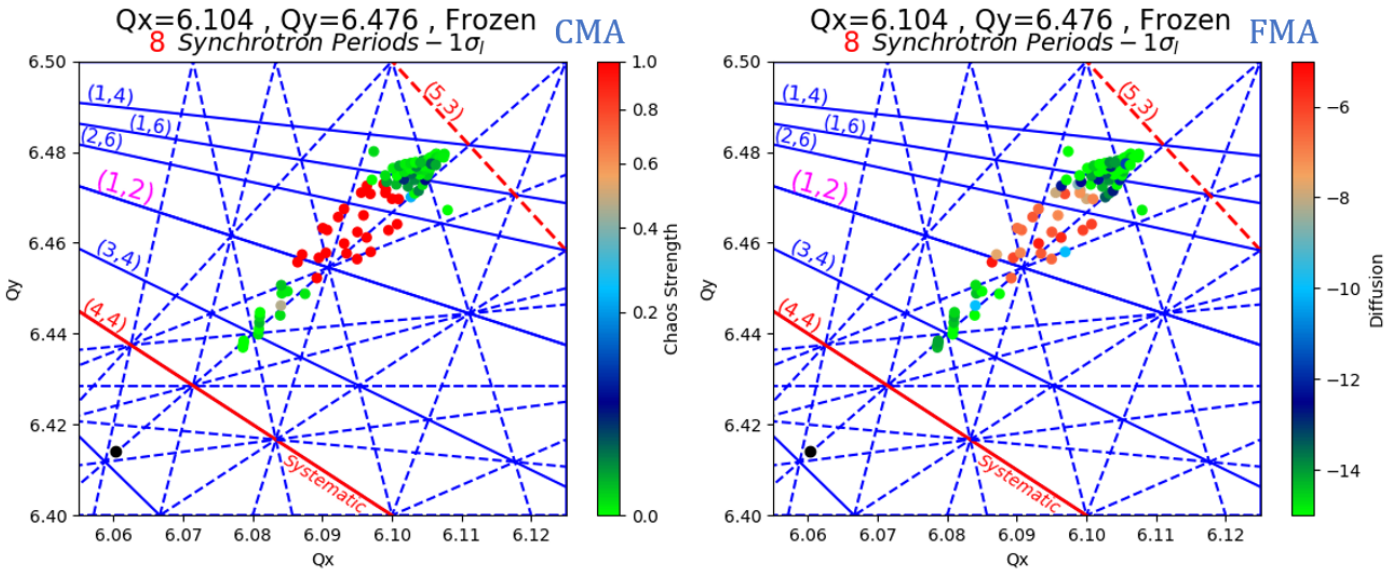

Figure 6.11: CMA and FMA footprints for $1\sigma_l$ - Frozen mode - Resonance tune.

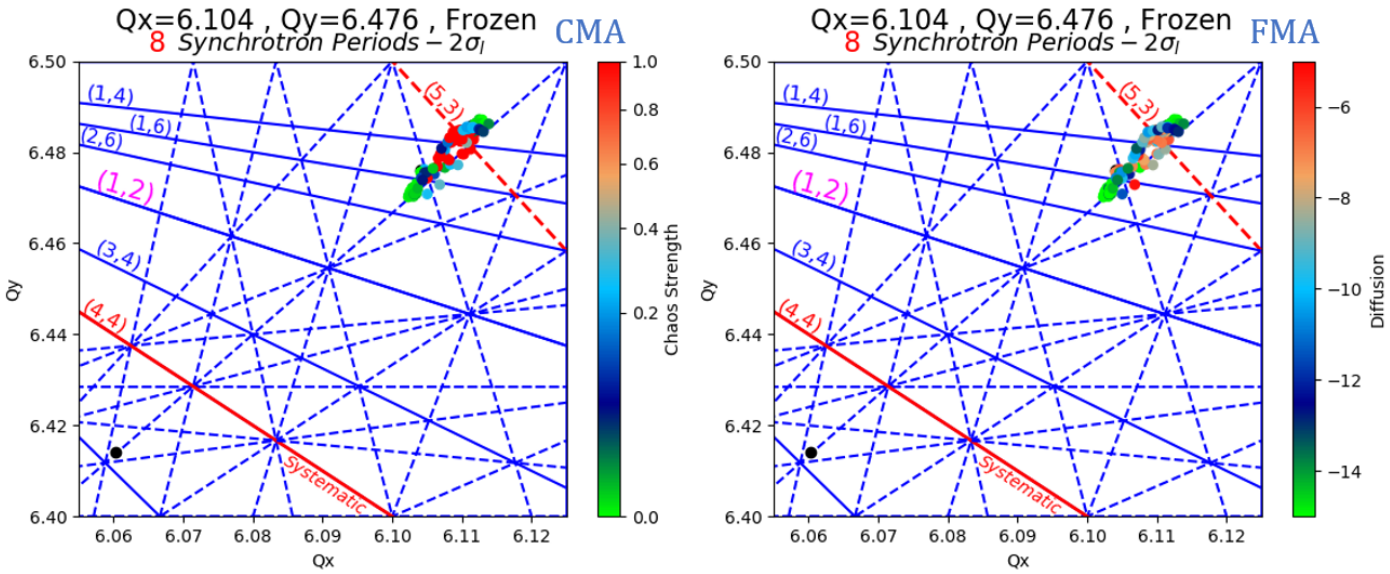

Figure 6.12: CMA and FMA footprints for $2\sigma_l$ - Frozen mode - Resonance tune.

6.3 Integer Tune

The last case that will be presented is the *integer tune* case which was the most difficult to analyze due to the very strong integer resonance. The data for this WP was analyzed many times, with different frequency windows of the frequency analysis due to numerical errors close to the integer resonance.

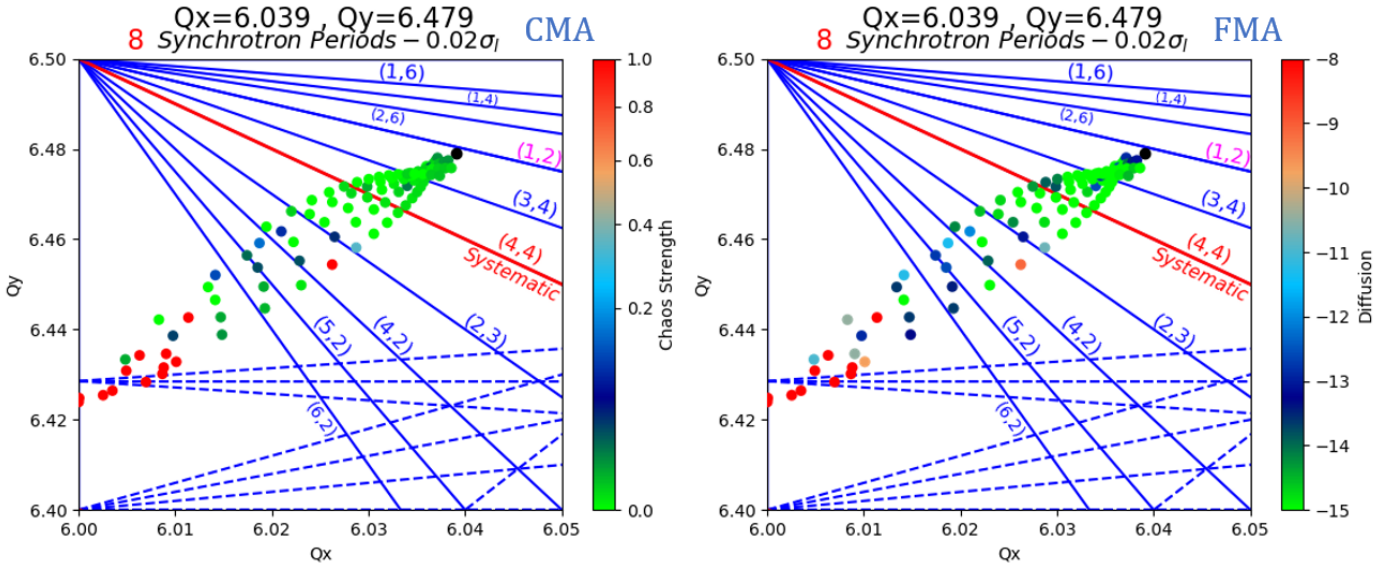

Figure 6.13: CMA and FMA footprints for $0.02\sigma_l$ - Integer tune.

Dealing with a WP that is close to the integer resonance is not trivial. For the on-momentum particles, the ones possessing large amplitudes and so are away from the integer resonance are expected to be stable or weakly chaotic. Though, particles with small amplitudes will be located close to the integer resonance due to the SC tune shift. These particles appear to be strongly chaotic and also the grid is deformed (see Fig. 6.13). Particles that appear to be on the integer resonance are possibly the result of numerical errors during the frequency analysis.

For the $1\sigma_l$ case, particles have larger frequencies and some of them are crossing the excited $(1, 2)$ resonance leading to strongly chaotic behaviour and particle spread in the tune diagram (see Fig. 6.14). Additionally, there are some strongly chaotic particles in the low amplitudes, too.

At the edge of the longitudinal distribution, most of the particles are located close to the $(1, 2)$ resonance leading to strongly chaotic motion (see Fig. 6.15). Individual particles that are located away from the majority are possibly the result of numerical errors or strong tune movement. For this WP, the results of both methods are again in agreement.

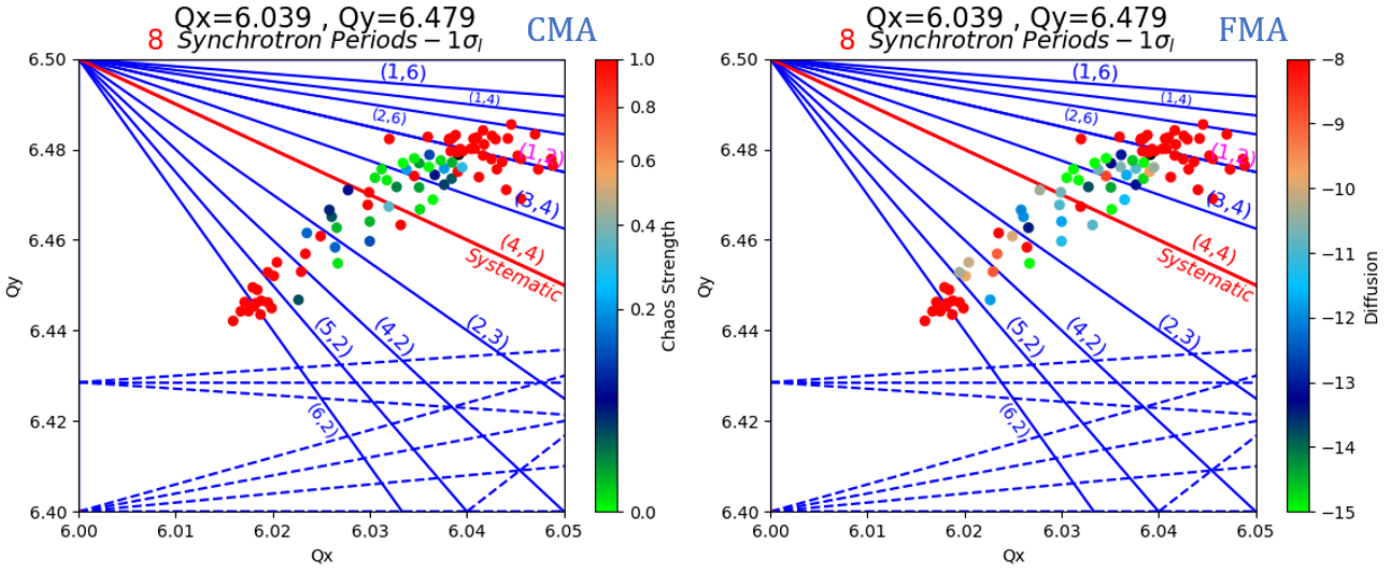

Figure 6.14: CMA and FMA footprints for $1\sigma_l$ - Integer tune.

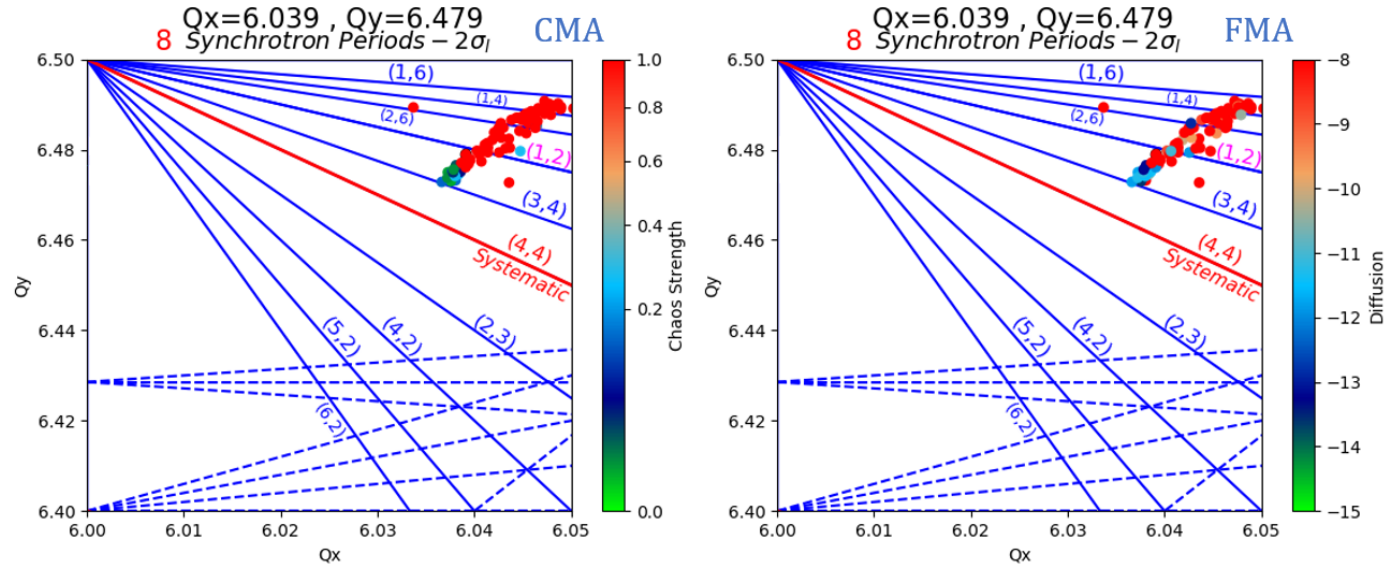

Figure 6.15: CMA and FMA footprints for $2\sigma_l$ - Integer tune.

7 Conclusions

The goal of this thesis was to review present tools (FMA) and a newly developed tool (CMA) in order to investigate particle stability in the PS, including SC. The combination of SC and lattice non-linear elements or imperfections can lead to chaotic motion withing the physical aperture of the beam which in turn will result in beam blow-up or particle loss.

The FMA is a method that evaluates the tune diffusion of the particles, while the CMA predicts if a particle exhibits regular or chaotic motion. In combination with the systematic way of the 6D phase space parametrization, the CMA method has to produce similar results to the one of the FMA.

As was previously shown, these two methods indeed agree with each other especially if we study cases with more than 7 synchrotron periods. For less periods, both methods seem to be slightly different but that should be overcome by fine-tuning of these techniques. Consequently, the CMA method is a nice tool to have in our toolbox.

The analysis of these tools indicate that the CMA method could be improved further. Both methods are further optimizing the tools and should eventually agree very close. In particular, the FMA technique now also uses the time evolution of the twin particles which originally are very close in phase space. Therefore, both methods now use the microscopic nature of either regular or chaotic motion.

Appendix A : Benchmarking Plots

Plots walk through

In the figures that are presented in this study various features have to be explained. To begin with, on the title are shown the WP, over how many synchrotron periods the results are evaluated and last, the sigma of the longitudinal distribution.

As was shown in Section 2.2, the lines in the tune diagrams represent the resonances. The blue lines are for non-systematic resonances while the red lines are for systematic resonances. Systematic resonances are much more dangerous for particle stability since the resonance condition is fulfilled for each optics period which is 50 in the case of PS. Additionaly, the full lines stand for normal up-right resonances while the dashed lines stand for skew resonances that are excited from skew magnetic components, e.g. a rotated sextupole. The type of each resonance is shown in the parenthesis.

Another feature of these plots is that the highest black dot, which is not visible in the plots below, is the WP of the specific case while the lowest black dot is the maximum SC tune shift. Also, in the smaller σ_l cases, as will be shown in some plots, the particles sit on a perfect grid. In that grid, the lower side is the emittance-ration-angle $\phi = 15°$ while the higher side is the angle $\phi = 75°$. The distance between each arc is roughly 0.5σ.

Additionally, in the CMA case the color-bar represents the chaos strenght while in the FMA the color-bar represents the diffusion. Notice that is the former case, the color-bar scale is not symmetrical. This way, the colors are further optimized to match better for both cases.

In the next pages, all the plots that were done for the benchmarking of the CMA method will be shown. The data that will be presented are from 1 full synchrotron period to 8 full synchrotron periods and are for a specific case of the PS in which the differences between the synchrotron periods are easily noticeable.

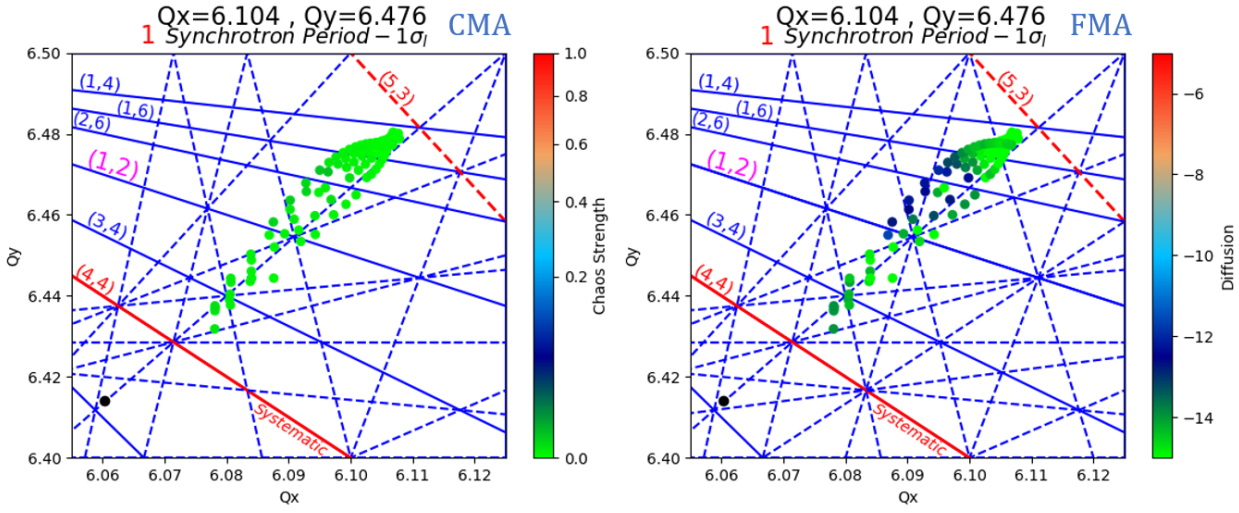

Figure A.1: Comparison of CMA and FMA over 1 full synchrotron period.

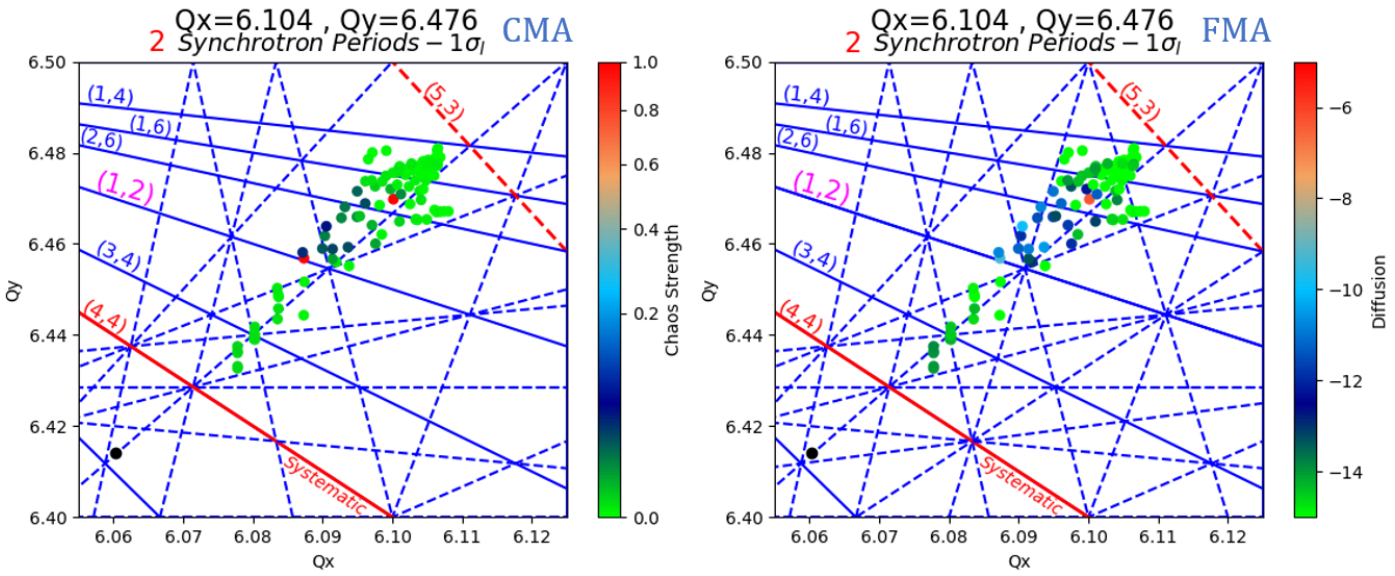

Figure A.2: Comparison of CMA and FMA over 2 full synchrotron periods.

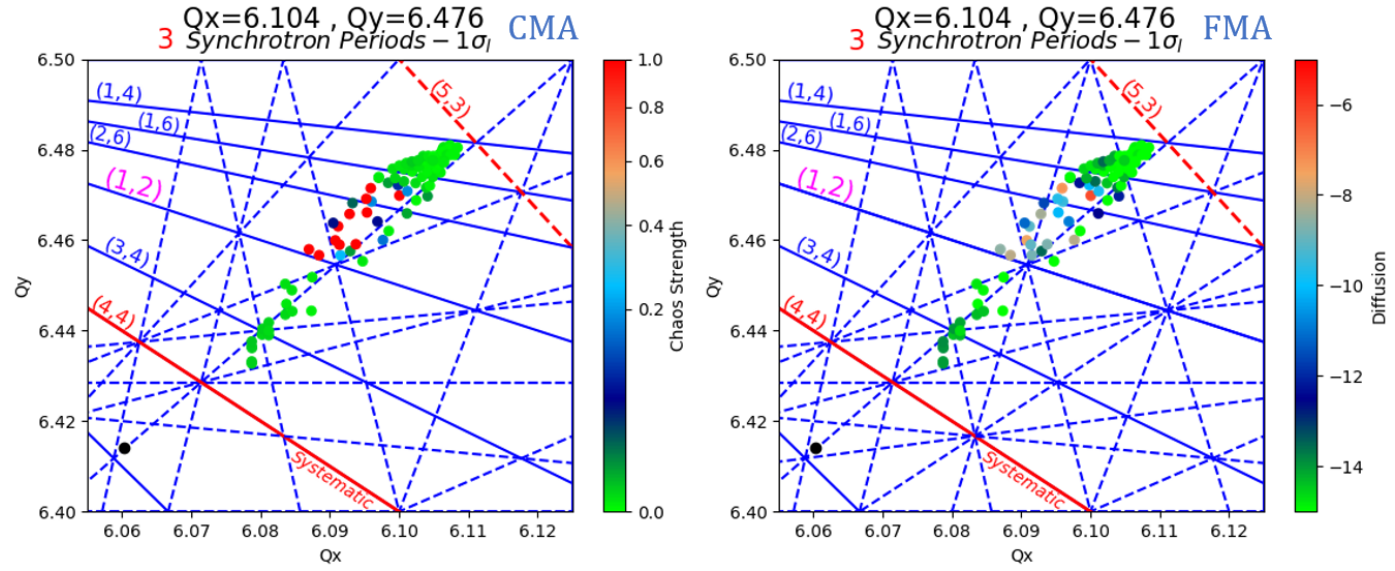

Figure A.3: Comparison of CMA and FMA over 3 full synchrotron periods.

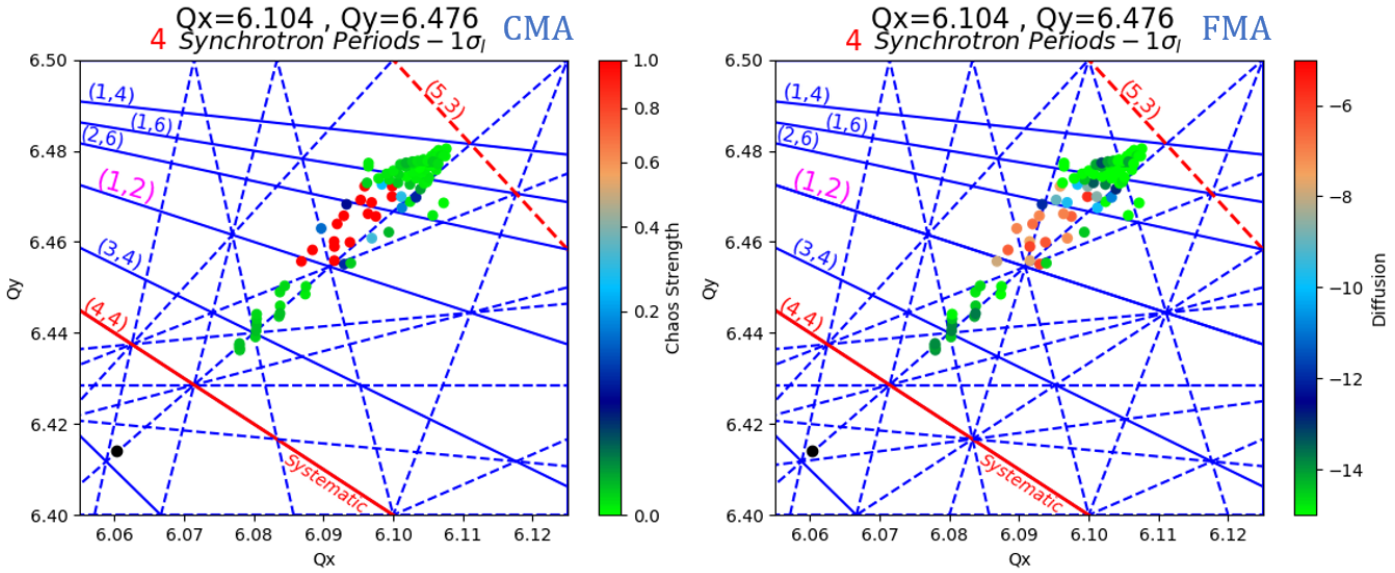

Figure A.4: Comparison of CMA and FMA over 4 full synchrotron periods.

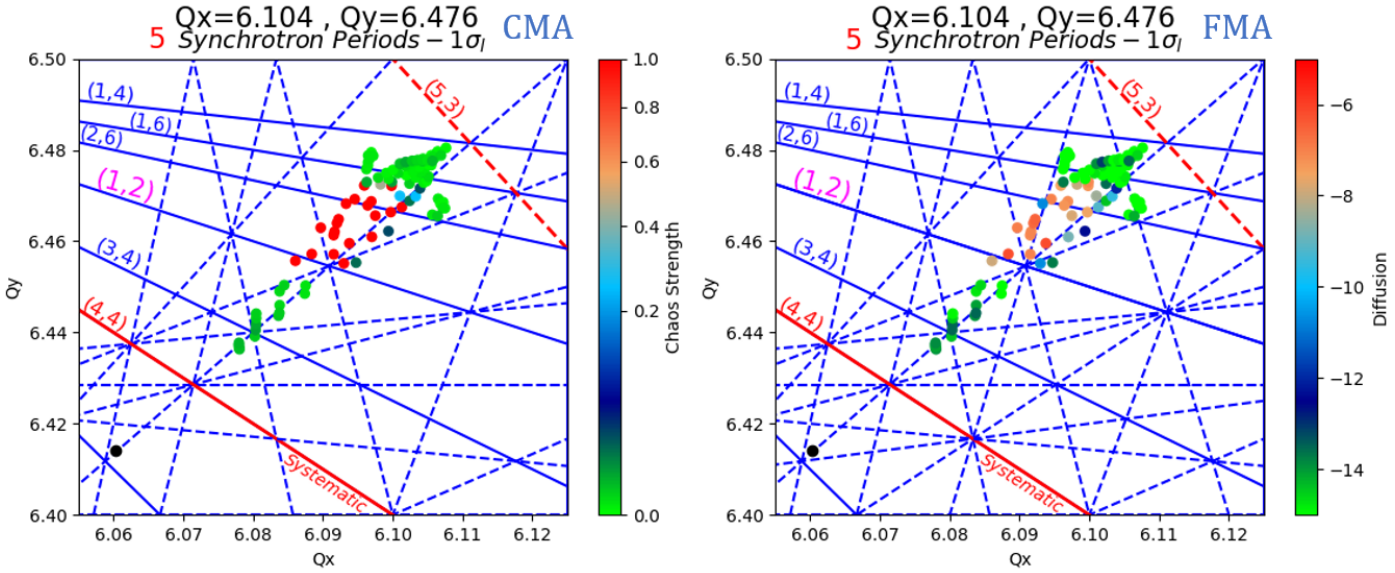

Figure A.5: Comparison of CMA and FMA over 5 full synchrotron periods.

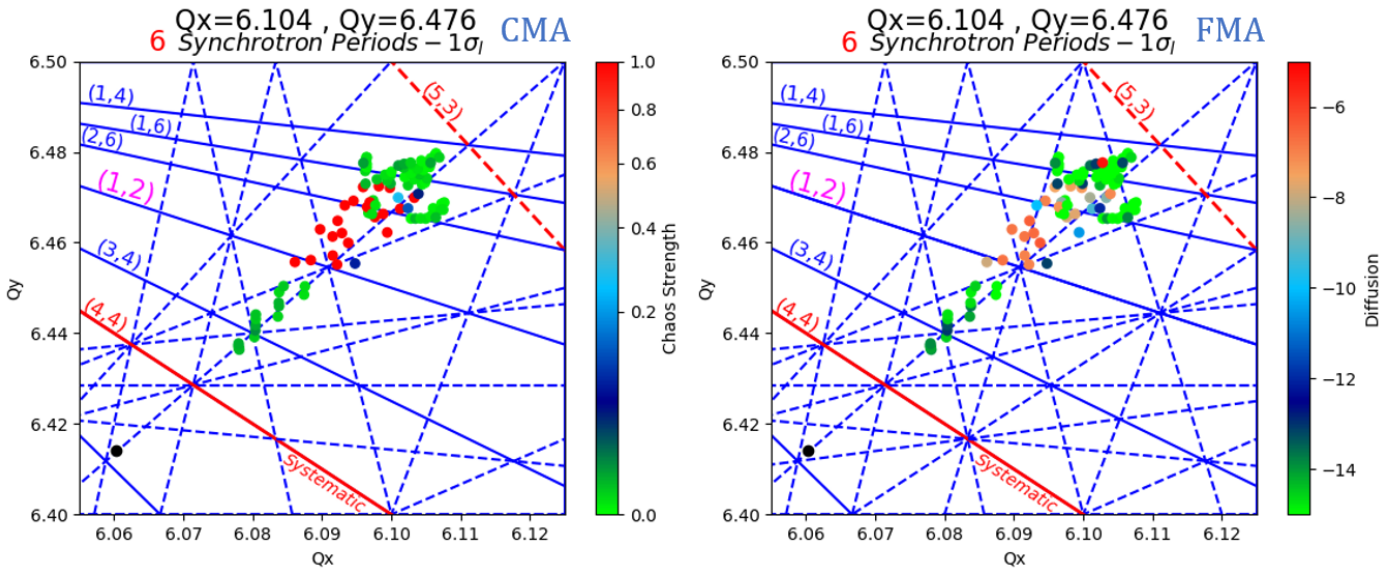

Figure A.6: Comparison of CMA and FMA over 6 full synchrotron periods.

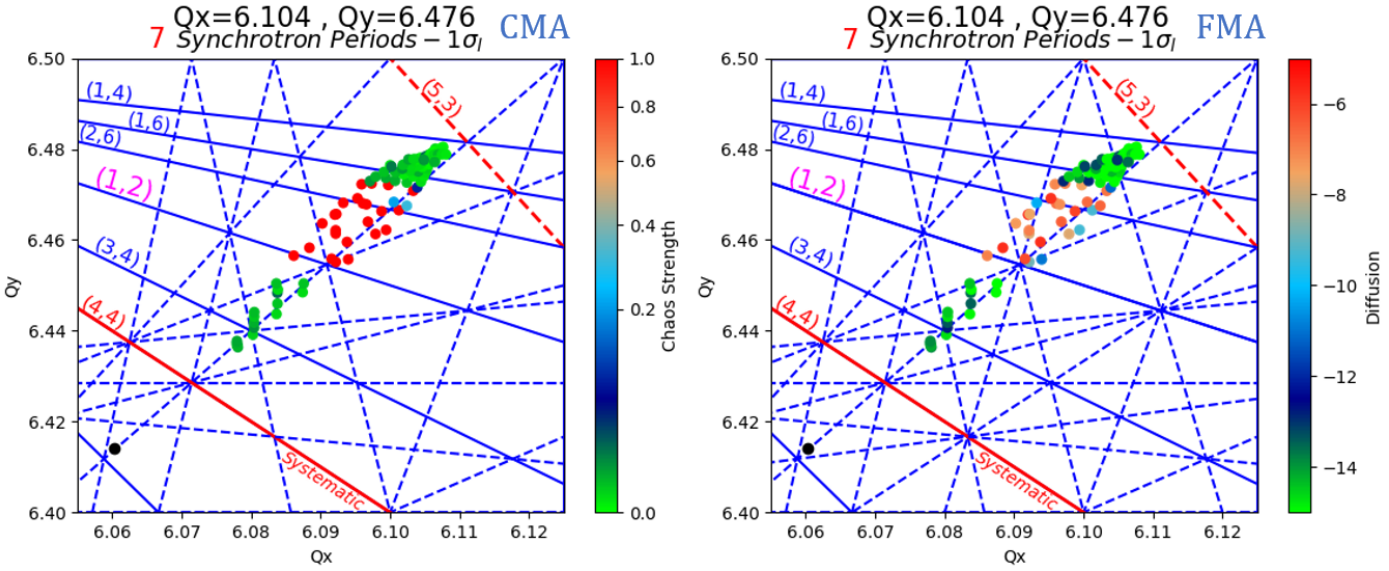

Figure A.7: Comparison of CMA and FMA over 7 full synchrotron periods.

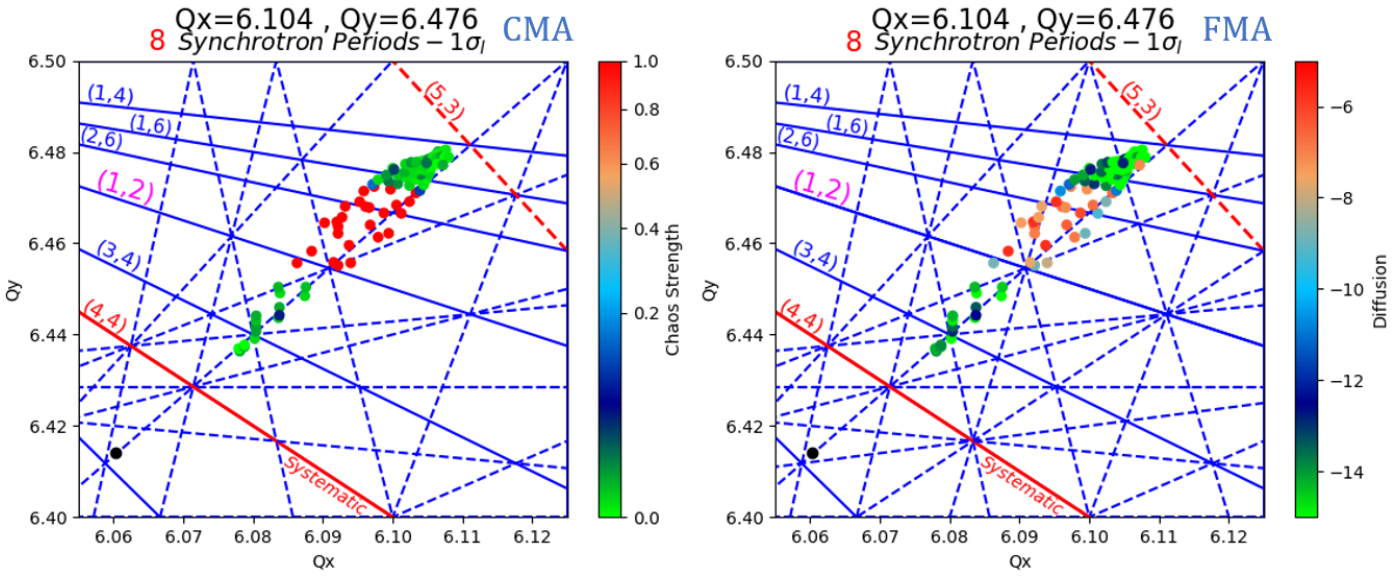

Figure A.8: Comparison of CMA and FMA over 8 full synchrotron periods.

For 1 synchrotron period there are no strongly chaotic particles in agreement with FMA where some particles show a little higher diffusion but still, their diffusion coefficients are small (see Fig. A.1). For 2 synchrotron periods some strongly chaotic particles appear reluctantly, accompanied by some weakly chaotic particles (see Fig. A.2). Increasing the number of synchrotron periods, the number of the chaotic particles increases in agreement again with FMA which shows large diffusion areas wherever we have strong chaotic areas. Even though the FMA seems to be more sensitive for small number of synchrotron periods, the results of the CMA technique seem to converge faster.

References

[1] B. V. Chirikov, *'A universal instability of many-dimensional oscillator systems'*, Physics reports, vol. 52, No. 5, pp. 263–379, 1979.
Available at:
http://lptms.u-psud.fr/nicolas_pavloff/files/2010/03/chirikov1.pdf

[2] R. D. Ruth, *'Single particle dynamics and nonlinear resonances in circular accelerators'*, Lecture Notes in Physics, Berlin Springer Verlag, vol. 247, Pages 37-63, 1986.
Available at:
http://www.slac.stanford.edu/pubs/slacpubs/3750/slac-pub-3836.pdf

[3] J. Rossbach, P. Schmüser, *'Basic course on accelerator optics'*, CAS Jyväskylä 1992 CERN 94-01, p. 76.
Available at:
https://cds.cern.ch/record/247501/files/p17.pdf

[4] G. Guinard, *'A general treatment of resonances in accelerators'*, Lectures given in the Academic Training Programme of CERN, Geneva 1978.
Available at:
https://cds.cern.ch/record/132991

[5] K. Schnindl, *'Space charge'*, CERN, Geneva 2006.
Available at:
http://cds.cern.ch/record/941316

[6] H. Bartosik, *'Space charge effects I: direct space charge'*, Presentation, 09/07/2015.
Available at:
http://frs.web.cern.ch/frs/Source/space_charge/Meetings/meeting61_09.07.2015/HB_Space_Charge.pdf

[7] H. J. Korsch, *'Nonlinear Dynamics and Deterministic Chaos'*, Chaos: A Program Collection for the PC, Springer Berlin Heidelberg, Pages 11-44, Berlin, Heidelberg, 1999.
Available at:
https://doi.org/10.1007/978-3-662-03866-6_2

[8] J. Laskar, *'Frequency analysis for multi-dimensional systems. Global dynamics and diffusion'*, Physica D: Nonlinear Phenomena, Volume 67, Issues 1-3, 1993, Pages 257-281, ISSN 0167-2789.
Available at:
http://www.sciencedirect.com/science/article/pii/016727899390210R

[9] J. Laskar, C. Froeschlé, A. Celletti, *'The measure of chaos by the numerical analysis of the fundamental frequencies. Application to the standard mapping'*, Physica D: Nonlinear Phenomena, Volume 56, number 2, 1992, Pages 253-269, ISSN 0167-2789.
Available at:
http://www.sciencedirect.com/science/article/pii/016727899290028L

[10] J. Laskar, *'Frequency map analysis and particle accelerators'*, Volume 1, 2003, Pages 378-382, 10.1109/PAC.2003.1288929.
Available at:
http://www.cpt.univ-mrs.fr/~hscopp04/Abstracts/Laskar.pdf

[11] Y. Papaphilippou, *'Detecting chaos in particle accelerators through the frequency map analysis method'*, Chaos: An Interdisciplinary Journal of Nonlinear Science, Volume 24, number 2, 2014, Pages 253-269, ISSN 0167-2789.
Available at:
`https://doi.org/10.1063/1.4884495`

[12] F.Asvesta, H.Bartosik, Y. Papaphilippou, M.Serluca, G.Sterbini *'Frequency Map Analysis in the PS'*, Space Charge Working Group Presentation, 13/7/2017.
Available at:
`https://indico.cern.ch/event/704697/contributions/2890996/attachments/1598026/2532293/fmas_97scwg.pdf`

[13] G. Franchetti, S. Gilardoni, A. Huschauer, F. Schmidt, R. Wasef, *'Space charge effects on the third order coupled resonance'*, American Physical Society: Phys. Rev. Accel. Beams, Volume 20, Issue 8, 2017.
Available at:
`https://cds.cern.ch/record/2286278/files/10.1103_PhysRevAccelBeams.20.081006.pdf`

[14] H. Grote, F. Schmidt, L. Deniau, G. Roy, *'The MAD-X Program: User's Reference Manual'*, CERN, 2016.
Available at:
`http://mad.web.cern.ch/mad/releases/5.02.08/madxuguide.pdf`

[15] R. Bartolini, F. Schmidt, *'SUSSIX: A Computer Code for Frequency Analysis of Non–Linear Betatron Motion'*, CERN SL/Note 98-017 (AP), 1998.
Available at:
`https://cds.cern.ch/record/702438/files/sl-note-98-017.pdf`

[16] F. Galluccio, F. Schmidt, *'Towards a better understanting of slow particle losses in large hadron colliders'*, CERN SL/Note, 1991.
Available at:
`https://cds.cern.ch/record/231594/files/cer-000146045.pdf`

[17] F. Schmidt, *'Untersuchungen zur dynamischen Akzenptanz von Protonenbeschleunigern und ihre Begrenzung durch chaotische Bewegung'*, Ph.D. Thesis, University of Hamburg, DESY HERA 88-02 (1988).